Publications of the Astronomical Society of the Pacific, 137:104504 (22pp), 2025 October https://doi.org/10.1088/1538-3873/ae0afe

Aligned, Multiple-transient Events in the First Palomar Sky Survey

Beatriz Villarroel[1], Enrique Solano[2,3], Hichem Guergouri[4], Alina Streblyanska[5], Stephen Bruehl[6], Vitaly M. Andruk[7], Lars Mattsson[1], Rudolf E. Bär[8], Jamal Mimouni[9], Stefan Geier[5,10], Alok C. Gupta[11], Vanessa Okororie[12], Khaoula Laggoune[13], Matthew E. Shultz[14], and Robert A. Freitas, Jr.[15]

[1] Nordita, KTH Royal Institute of Technology and Stockholm University, Hannes Alfvéns väg 12, SE-106 91 Stockholm, Sweden
[2] Departamento de Astrofísica, Centro de Astrobiología (CSIC/INTA), PO Box 78, E-28691, Villanueva de la Cañada, Spain
[3] Spanish Virtual Observatory, Spain
[4] Science of the Matter Division. Research Unit in Scientific Mediation, CERIST, Constantine, Algeria
[5] Instituto de Astrofísica de Canarias, Avda Vía Láctea S/N, La Laguna, E-38205, Tenerife, Spain
[6] Department of Anesthesiology, Vanderbilt University Medical Center, 701 Medical Arts Building, 1211 Twenty-First Avenue South, Nashville, TN 37212, USA
[7] Main Astronomical Observatory Observatory of the NAS of Ukraine, 27, Akademika Zabolotnoho St., Kyiv, 03143, Ukraine
[8] Institute for Particle Physics and Astrophysics, ETH Zurich, Wolfgang-Pauli-Strasse 27, CH-8093 Zurich, Switzerland
[9] Department of Physics, University of Constantine-1, LPMPS & CERIST, Constantine, Algeria
[10] Gran Telescopio Canarias (GRANTECAN), Cuesta de San José s/n, 38712 Breña Baja, La Palma, Spain
[11] Aryabhatta Research Institute of Observational Sciences (ARIES), Manora Peak, Nainital, 263 001, India
[12] Center for Basic Space Science, National Space Research and Development Agency, Enugu, Nigeria
[13] Sirius Astronomy Association, Algeria
[14] Department of Physics and Astronomy, University of Delaware, USA
[15] Institute for Molecular Manufacturing, Palo Alto, CA, USA
Received 2025 June 8; revised 2025 September 23; accepted 2025 September 24; published 2025 October 17

Abstract

Old, digitized astronomical images taken before the human spacefaring age offer a rare glimpse of the sky before the era of artificial satellites. In this paper, we present the first optical searches for artificial objects with high specular reflections near the Earth. We follow the method proposed in Villarroel et al. and use a transient sample drawn from Solano et al. We use images from the First Palomar Sky Survey to search for multiple (within a plate exposure) transients that, in addition to being point-like, are aligned along a narrow band. We provide a shortlist of the most promising candidate alignments, including one with $\sim 3.9\sigma$ statistical significance. These aligned transients remain difficult to explain with known phenomena, even if rare optical ghosting producing point-like sources cannot be fully excluded at present. We explore remaining possibilities, including fast reflections from highly reflective objects in geosynchronous orbit, or emissions from artificial sources high above Earth's atmosphere. We also find a highly significant ($\sim 22\sigma$) deficit of POSS-I transients within Earth's shadow when compared with the theoretical hemispheric shadow coverage at 42,164 km altitude. The deficit is still present though at reduced significance ($\sim 7.6\sigma$) when a more realistic plate-based coverage is considered. This study should be viewed as an initial exploration into the potential of archival photographic surveys to reveal transient phenomena, and we hope it motivates more systematic searches across historical data sets.

Unified Astronomy Thesaurus concepts: Search for extraterrestrial intelligence (2127); Transient detection (1957); Surveys (1671); Solar system astronomy (1529)

1. Introduction

Digitized sky surveys have broadened the time window in which we can study changes in the sky. Programs such as the Digital Access to a Sky Century at Harvard (DASCH; Grindlay et al. 2012), the Digital Sky Survey[16] (DSS), the Ukraine Virtual Observatory (JDA UkrVO; Vavilova et al. 2012; Vavilova et al. 2017), and *Carte du Ciel*, provide images of the sky spanning not just a few decades but, in some cases, over 150 yr.

While photographic plates are no longer used for large astronomical surveys—having been replaced by significantly faster and more sensitive CCDs—the archival images still serve important scientific purposes. For example, they allow studies of long-term variability of astronomical sources over timescales of decades or even a century, assuming the object is bright enough to be detected.

Another use of these archives is to search for vanishing stars and other transients. In the Vanishing and Appearing Sources during a Century of Observations (VASCO; Villarroel et al. 2016, 2020) project, images of the sky taken in the early

[16] https://archive.stsci.edu/cgi-bin/dss_form/

1950s, prior to the first anthropogenic satellite, are compared with modern surveys to identify possible sources that may have disappeared. VASCO employs two complementary approaches: first, an automated procedure (Solano et al. 2022) that searches digitized image data from the First and Second Palomar Sky Surveys (POSS-I and POSS-II) for transients; and second, a citizen science project (Villarroel et al. 2022b) where volunteers classify potentially interesting objects. These efforts are facilitated by the Spanish Virtual Observatory[17] and its software tools. The VASCO program has resulted in the cataloging of many thousands of unknown transients, visible only within a single plate exposure (Solano et al. 2022; Villarroel et al. 2022b).

An intriguing finding from the VASCO project was presented in Villarroel et al. (2021): nine faint, star-like objects that appeared and vanished simultaneously on a 1950s POSS-I plate. The central transient was first identified during the visual vetting of 24,000 candidates with small cutout images of fix size, yielding ∼100 vanishing star-candidates, see Table 2 of Villarroel et al. (2020). In a subsequent follow-up of these 100 transients, the image containing nine transients was discovered. The nine transients were not visible on another plate taken half an hour earlier, nor on a third plate six days later. All known astrophysical explanations were considered but deemed implausible. The surface density of such transients was too high to be attributed to any known natural phenomenon. Whether this was due to unknown contamination on the plate with coincidentally star-like defects or a genuine astronomical observation remains unresolved. If real, one explanation could be that they were caused by solar reflections off flat, highly reflective objects in geosynchronous orbit (GSO) around the Earth. Nevertheless, the nine transients on their own are ambiguous, particularly since they are located near the plate edge, where defects are known to accumulate (Hambly & Blair 2024) and where other round objects can also be found. Yet the finding prompts a provocative question: could some of the objects long dismissed as plate defects actually represent reflections or emissions from artificial sources? And, more generally, can pre-Sputnik plates serve as a search domain for non-human artificial objects?

Finding such objects in pre-Sputnik data, would represent a significant discovery with far-reaching implications for both astronomy and humanity, including the possibility of non-terrestrial artifacts (NTAs). It also bears directly on the scientific investigation of Unidentified Anomalous Phenomena (UAPs), formerly known as Unidentified Flying Objects ("UFOs")—a subject that, after decades of stigma, is now gaining serious academic attention, as highlighted in the recent review by Knuth et al. (2025) in *Progress in Aerospace*. Clarifying the origin of these transient events is therefore not only of astrophysical interest but also of potential importance for one of the most enigmatic and consequential questions facing science today.

To add to the intrigue, Solano et al. (2023) recently reported a bright triple transient event occurring on 1952 July 19, found among a set of ∼5000 short-lived POSS-I transients (Solano et al. 2022). This highly curated data set, in which diagnostics based on photometry and morphometric parameters have been carefully applied to the sample to reduce false positives (e.g., plate defects), suggests that the phenomenon of multiple transients can be found even when stringent diagnostic criteria are applied. As in the earlier case with the nine transients, the objects appeared and vanished within a single 50 minutes exposure. Their brightness ($r \sim$ 15–16 mag) makes contamination less likely. Notably, this particular event coincides in time with one of the most extensively documented aerial anomalies in historical records: the Washington D.C. "UFO flap" of 1952 July, which unfolded over two consecutive weekends (July 18–19 and 26–27). While this may be a coincidence, the temporal proximity invites further scrutiny—especially given the rarity of both phenomena. In a separate study Bruehl & Villarroel (2025), we investigate possible statistical associations between historical UAP reports and VASCO transients, and find preliminary evidence of a temporal correlation at the $\sim 3\sigma$ level. While such a finding does not imply causation, it raises the possibility that certain anomalous aerial observations recorded in the pre-satellite era may have had physical counterparts observable in deep-sky imaging.

Given the unusual nature and potential implications of these events, it is essential to test the hypothesis that some transients arise from reflective artificial objects in Earth orbit, and that certain point-like features long dismissed as plate defects may in fact be solar reflections from artificial surfaces. Searches for extraterrestrial probes were proposed as early as the 1960s (Bracewell 1960), but to date only a few searches for NTAs have been attempted or proposed (Freitas & Valdes 1980; Valdes & Freitas 1983; Freitas & Valdes 1985; Haqq-Misra & Kopparapu 2012).

In a previous white paper, Villarroel et al. (2022a) proposed a methodology to search for solar reflections from artificial objects in GSO using photographic plates from before the satellite era (pre-1957). One key signature is the presence of several point-like transients that are aligned along a line within a single exposure. A statistical framework was also developed to assess the significance of such alignments.

In this paper, we carry out that test. We apply the published methodology and statistical framework to a published sample of POSS-I transients from Solano et al. (2022).

We identify several promising candidates and examine them in detail in Section 5. Assuming the events are real, we use the aligned transients to infer the possible geometry and surface density of reflective objects near GSO. We also perform a statistical test to evaluate whether sunlight is required to

[17] http://svo.cab.inta-csic.es

produce these transients, based on their detection rate within Earth's shadow. Finally, we discuss prospects for detecting similar objects in modern digital sky surveys.

2. Plate Defect or Technosignature?

One of the core challenges in our work is the contamination of photographic plates by artifacts that may mimic astronomical sources. Apparent transient events in these plates often present a case of degeneracy—where genuine astrophysical signals and mundane defects can appear strikingly similar. Certain plate defects are known to resemble stellar profiles (Greiner et al. 1990), and distinguishing them from authentic observations remains a nontrivial task, even when full-width-half-maximum (FWHM) comparisons are applied. Moreover, defects can cluster near plate edges, and vignetting or uneven development may further confound interpretation. Nevertheless, visual inspection and photometric profile analysis remain indispensable tools in this early phase of exploration.

Rigorous diagnostics with quantitative measurements are central to any search for genuine transients in photographic plates, as overly permissive criteria inevitably admit large amounts of noise. For that reason, we shall use carefully selected transient samples in Solano et al. (2022), which average 167 transients per plate and have been matched to several modern surveys to remove variable stars, asteroids, and comets.

It is scientifically untenable to assume that all candidates are either authentic transients or all defects. A reasonable working assumption is that both populations are present in some unknown proportion. From this perspective, even a single authentic detection among many contaminants would validate the effort and warrant continued search.

This degeneracy is intrinsic to any attempt at identifying NTAs in archival material. Two primary examples illustrate this problem:

1. *Narrower FWHMs and rounder profiles.* Hambly & Blair (2024) interpret slightly more concentrated, round profiles as signs of spurious detections and makes an example with Villarroel et al. (2021). However, atmospheric seeing and short-lived (sub-second to few-second) optical events are also expected to produce narrower FWHMs than long-exposed stars (Tokovinin 2002; Villarroel et al. 2025a). Thus, profile sharpness alone cannot conclusively distinguish between artifact and astrophysical origin. We note, in passing, that Hambly & Blair (2024) have not attempted to apply their analysis to the triple transient reported by Solano et al. (2023), which might have provided a more stringent test of their conclusions.
2. *Spatial distributions.* A high number density of transient-like features in one region could be mistaken for evidence of poor plate quality. But the number density of transients on a plate is not diagnostic. If NTAs exist in coordinated swarms, these swarms could span tens of square degrees, easily covering entire plates, while a grid of NTAs could cover the entire sky.[18] In ambiguous and uncertain cases—such as the plate analyzed in Villarroel et al. (2021)—additional transients or artifacts may surround the nine candidates (see Supplementary Information of mentioned paper). Their presence illustrates the degeneracy problem: authentic events may coexist on the same plate as numerous star-like defects, which makes it essential to apply independent diagnostics such as alignment statistics and Earth's shadow tests.

Because of the ambiguity in these early cases, we advocated for more targeted searches in Villarroel et al. (2022a), emphasizing particularly multiple transients aligned along a line—where statistical analysis can decisively test whether such configurations occur by chance.

Moreover, the temporal correlations between the 1950s transients and both the Washington 1952 UFO events and 124 U.S., Soviet, and British nuclear weapons tests deserve serious attention. Even if individual events remain uncertain, Bruehl & Villarroel (2025) shows statistically significant correlations between subsets of the transient sample in Solano et al. (2022) and historical nuclear activity and aerial anomalies. This alone contradicts the idea that the entire sample consists of plate defects.

Finally, one of the most revealing tests involves Earth's shadow. No matter how asymmetric or irregular the distributions of plate defects may be, they have no plausible reason to avoid the Earth's shadow. In contrast, transients associated with solar reflections would. This shadow test provides a crucial empirical lever to distinguish between physical reflections and random defects—and remains an essential part of any validation framework moving forward.

In this paper, we rely on hypothesis testing across large samples—assessing statistical correlations, spatial alignments, and Earth-shadow sensitivity—offering a robust framework that remains valid even in the presence of substantial stellar-like contamination. In the future, we aim to use AI-driven methods to filter out transients that resemble plate defects or occur in problematic regions of the plates, and to establish an upper limit on the fraction of objects that may represent NTAs. For now, we will use the simplest methods to search for candidates that show signs of solar reflection.

[18] See e.g., Patrick Jackson's sphere network: https://www.amazon.com/Sphere-Network-Mr-Patrick-Jackson/dp/B0DXF1RGL6.

3. Predictions and Expectations

Natural transients occur at a rate several orders of magnitude lower than glints from artificial objects. Even detecting two natural transients within a few arcminutes of each other during a one-hour exposure is extremely unlikely.[19]

In contrast, glints caused by solar reflections from flat, highly reflective surfaces at high altitudes—such as GSOs—could result in multiple, simultaneous point-like transients during a single long-exposure image. If the glints originate from the same object, they may appear aligned along a narrow band or straight line. In simple geometries, the glints could be equidistant and of similar brightness. However, more complex surface structures may lead to irregular spacing and variable flux (e.g., Nir et al. 2021; Villarroel et al. 2022a). Also objects flying in formation or coordinated swarms, might be found along geometric patterns.

Multiple transients in a single image are frequently detected in modern automated surveys. Nearly all transients with durations shorter than 0.5 s are caused by this phenomenon, often originating from satellites or space debris (e.g., Corbett et al. 2020; Nir et al. 2021). These events typically have apparent magnitudes of $r \sim 9$–11. The rate of such artificial glints can reach $\sim$1800 events hr^{-1} sky^{-1} near the equator (Corbett et al. 2020), which would overwhelm any comparable phenomena in modern surveys unless specifically targeted. The red POSS-I plates, reaching $r \sim 20$ mag with $\sim$50 minutes exposures, are still capable of detecting glints as short as 0.5 s, although the flux is diluted by approximately 9 mag.

Plate defects, by contrast, are expected to be randomly shaped and distributed. The chance that several defects simultaneously mimic star-like point sources and align along a narrow band is small. The method proposed in Villarroel et al. (2022a) identifies "simultaneous transients" that appear within the same long-exposure photographic plate and are additionally aligned within a narrow tolerance. This alignment criterion helps distinguish potentially artificial signals from random celestial or instrumental sources.

For example, an image with nine transients inside a 10×10 arcmin^2 box may exhibit a 4-point or 5-point alignment, with a statistical significance between 2.5σ and 3.9σ depending on the geometry. For exact probabilities, we refer the reader to Section 5 in Villarroel et al. (2022a), which uses the statistical framework developed by Edmunds (1981), Edmunds & George (1985). Even 3-point alignments may be considered when the total number of transients in a region is low. Alignments with the lowest probability of occurring by chance should be prioritized for further examination, though not interpreted as conclusive evidence of geosynchronous reflections.

Taken together, these considerations show that the occurrence of aligned, simultaneous transients on photographic plates is an excellent candidate signature of reflective orbital objects, especially in the absence of natural or instrumental explanations.

While alignments of multiple transients provide a statistically robust signature, it is important to note that most glints caused by solar reflections are expected to appear as single, isolated transients on a photographic plate. This follows naturally from the geometry of specular reflection, where a glint is only visible when the orientation of a rotating object briefly aligns with the observer and the Sun. Assuming a large population of such objects in geosynchronous or higher orbits, the majority of events will not repeat and will appear on a single plate only. These point-like flashes may still exhibit perfect PSF shapes and are typically absent in Earth's shadow, further distinguishing them from both natural and instrumental phenomena. Although individual transients carry less statistical weight, the overall rate and behavior of such events can still be used to identify a non-natural origin. As shown in Villarroel et al. (2022a), statistical models incorporating both aligned and non-aligned transients offer complementary routes for detecting technosignatures in historical data.

4. Methods and Selection

We base our analysis on the catalog of 298,165 short-duration transients presented in Solano et al. (2022), detected in red POSS-I plates with typical exposure times of 45–50 minutes. These transients were identified using an automated pipeline developed as part of the VASCO project. For full details on the detection methodology, data characteristics, and vetting steps, we refer readers to Solano et al. (2022).

From this data set, we search for spatial groupings of transients within square boxes of varying sizes, typically ranging from a few arcminutes up to 20′–30′ per side (see typical sizes in Table 2). For each group, we evaluate whether the positions of the transients fall along a straight line (or more precisely a narrow band), within astrometric uncertainties.

We quantify the degree of alignment using the Pearson correlation coefficient α between right ascension and declination. We retain only those candidate alignments where $|\alpha| > 0.99$. We note that the correlation is computed without applying a $\cos(\delta)$ correction to right ascension. Given the small angular separations involved, this has a negligible effect on the ranking of candidate alignments.

Table 1 summarizes the number of aligned groups found with $r \geqslant 3$, $r \geqslant 4$, $r \geqslant 5$, and $r \geqslant 6$ transients, respectively. Because the search boxes vary in size, the number of transients per group is not directly comparable across cases.

[19] We consider the probability of detecting a transient within 1 hr in the POSS-I survey, based on Solano et al. (2022), who identified 298,000 transients over 780 hr of exposure. The chance of finding one transient in a 10 arcmin^2 box in one hour is approximately $\sim$0.0016. The probability of two such transients appearing in the same box is then $p \sim 10^{-6}$.

Table 1
Candidates

Region	$r \geqslant 3$	$r \geqslant 4$	$r \geqslant 5$	$r \geqslant 6$
$0 <$ R.A. $< 100,\ 0 <$ decl. < 90	22	5	⋯	⋯
$100 <$ R.A. $< 200,\ 0 <$ decl. < 90	18	7	⋯	⋯
$200 <$ R.A. $< 300,\ 0 <$ decl. < 90	32	6	1	⋯
$300 <$ R.A. $< 360,\ 0 <$ decl. < 90	11	2	1	⋯
Total	83	20	2	0

Note. Total number of aligned transient candidates identified in each sky region. r is the number of aligned points. Note that $r \geqslant 4$ and $r \geqslant 5$ are subsets of $r \geqslant 3$. R.A. and decl. are in degrees.

All 83 candidates are presented in the Appendix. Visual inspection reveals that duplets and triplets are relatively common. However, rather than evaluate every alignment with $N \geqslant 3$, we focus on higher-confidence candidates with at least four aligned transients.

Many POSS-I plates have been scanned by both DSS and the SuperCOSMOS Sky Survey (Hambly et al. 2001). Since SuperCOSMOS images generally offer higher spatial resolution, we used both sources to verify each alignment. We downloaded FITS images for all candidates with $N \geqslant 4$, selecting image boxes that encompass the full alignment.

In several cases, transients initially appearing as point sources in DSS were revealed—through SuperCOSMOS images—to be either scanning artifacts or round defects likely caused by emulsion flaws. Transients absent from the higher-resolution scan were excluded from further consideration. We thus retained only those candidates that:

1. Show at least four star-like transients in a roughly linear arrangement on the DSS scan;
2. Are confirmed by the corresponding SuperCOSMOS scan. The DSS and SuperCOSMOS scans are independent digitizations of the same physical photographic plate, obtained using different scanners, optics, and digitization procedures. This means that any object visible in both scans is almost certainly a real feature present on the plate emulsion. In contrast, an object visible in only one of the scans is most likely a scanning artifact caused by dust on the scanner glass, digitization noise, or compression effects—not a genuine plate defect. We therefore treat agreement between both scans as a strong indicator of authenticity. Furthermore, we note that some objects that initially appear point-like in DSS images may exhibit subtle asymmetries or deviate from a stellar PSF in the higher-resolution SuperCOSMOS images, leading us to reject them. This procedure helps ensure that the remaining candidates are not spurious artifacts introduced during digitization.

From this refined set, we identify five of the most promising candidates in the northern hemisphere, listed in Table 2.

There are two key ways the search procedure could be improved:

1. *Search area.* Objects in GSO move at $\sim 10''\ \mathrm{s}^{-1}$, or about 10° during a 50 minutes exposure. Our current box size (up to $30'$) is conservative and may miss longer alignments.
2. *Correlation threshold.* The criterion $|\alpha| > 0.99$ is unnecessarily strict and excludes mildly curved or non-ideal alignments.

However, relaxing either parameter would drastically increase the number of candidates—potentially into the tens of thousands—necessitating substantial manual vetting. To address this, we are developing an expansion of the VASCO citizen science platform (Villarroel et al. 2022b) tailored to this task.

5. The Shortlist

The shortlist in Table 2 shows the candidates. Each candidate is shown in Figures 1–5. Here we show only the transients themselves to assist the reader. The same images, but showing the actual alignments, can be found in Figures 6–10. The alignments differ in width; therefore, a dashed double line is shown in some particular cases where the width of the stripe is larger than $1''$.

In some cases—for example, the objects marked with crosses in Candidate 3 and Candidate 5—it is not certain that every transient is a point source, based on inspection of the images. Slight asymmetries in the light profiles are present in a few cases, manifesting as mild elongations (from e.g., movement) or qualitative irregularities in shape.[20] Therefore, the alignment is possibly a combination of transients and plate defects—or objects in the sky within our atmosphere. The reader can inspect the high-resolution images from SuperCosmos.[21] We improve the astrometry for the images using the Terapix *SWarp* procedure. We measure the improved coordinates and the FWHM for each transient; see Table 3. The dates are taken from the STScI DSS Plate Server.

In a few cases, it is possible to derive more than one variant of the alignment—for example, with either a 3-point or a 4-point alignment. In such cases, we show both options separately in the images in Figures 6–10. For the cases in the shortlist, we estimate the probability of a chance alignment; see Section 6.

[20] These asymmetries refer to deviations in morphology, not to the full width at half maximum (FWHM), which varies across the plates due to well-documented instrumental and photochemical effects. As discussed in Villarroel et al. (2025a), the nonlinear response of photographic emulsions causes brighter objects to naturally appear with broader profiles, contributing to the observed FWHM spread.

[21] http://www-wfau.roe.ac.uk/sss/pixel.html

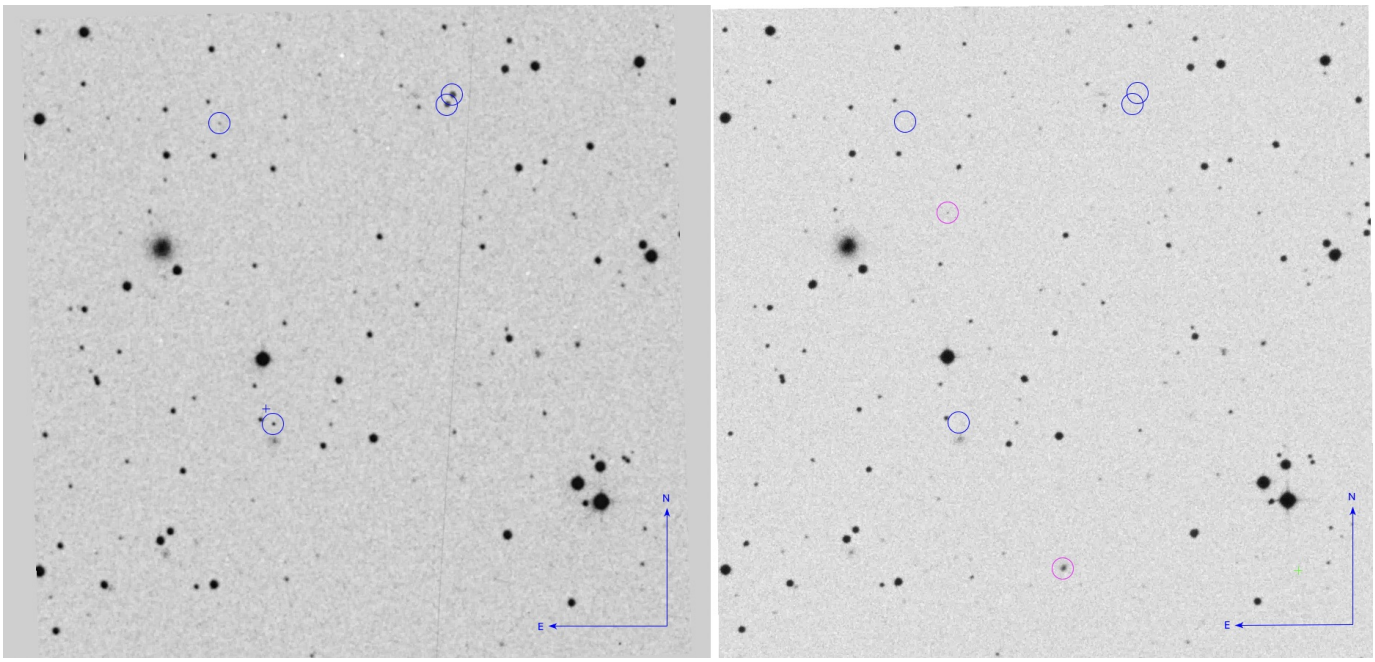

Figure 1. Candidate 1. We show the candidate in SuperCosmos scans of POSS-I red (left) and POSS-II red (right) images (inverted). Transients are marked with blue circles. The candidate with a measured coordinate is marked with a cross (+). Pink circles show defects. Also the gray line crossing the POSS-I field is a scanning defect. Four transients are visible in the POSS-I image, where three follow a straight line. Box size is 10×10 arcmin^2. See Figure 6 for a version with drawn lines that shows the possible alignment.

Table 2
Candidate Shortlist

Candidate Shortlist									
Candidate	Year	R.A. Decl. (sexag., J2000)	R.A. Decl. (deg, J2000)	r	N	A (arcmin^2)	$p_{\max}$ (arcsec)	$d_{\max}$ (arcmin)	μ_r
1	1954	02:29:33.71 +28:31:56.98	37.3904454 28.5324936	3	4	10×10	1.0	5.8	0.044
2	1955	03:05:42.48 +07:58:29.60	46.4269814 7.9748892	3	5	10×10	1.0	3.6	0.010
3	1954	03:08:27.13 +34:40:46.01	47.1130236 34.6794470	3	5	15×15–16	2.0	9.9	0.194
”	”	””	”	5*	5	”	15.0	”	0.002
4	1954	21:24:39.71 +68:31:30.04	321.1654740 68.5250111	3	6	12×12	1.0	5.15	0.049
”	…	”	”	4*	6	”	5.0	”	0.003
5	1952	19:16:45.76 +51:28:52.40	289.1906854 51.4812217	3	5	10×10	1.0	4.0	0.028
”	…	”	”	5*	5	10×10	10.0	4.0	0.0001

Note. We show the most interesting candidates emerging after the visual inspection. In some cases there could be different possibilities of r-point alignments, e.g., $r = 3$ or $r = 4$, and we show both possibilities marked by an asterisk (*). The given position coordinate corresponds to the transient marked with a cross (+) in each figure.

6. Statistics

The section below provides a brief recapture of the statistical framework developed in Section 5 of Villarroel et al. (2022a), where interested readers can explore the details of the framework. It builds on Edmunds (1981) and Edmunds & George (1985) which criticized Halton Arp's quasar alignments. The common critique was that with a large number density of objects, alignments will inevitably appear. These papers developed a statistical framework to investigate the actual probability of chance alignments.

For each of the interesting cases we consider the total number N of transient-like objects found in the image field, i.e., the area A of the image, and look for r objects aligned within a strip of width $p_{\max}$ and length $d_{\max}$. Such alignments will be referred to as r-point alignments.

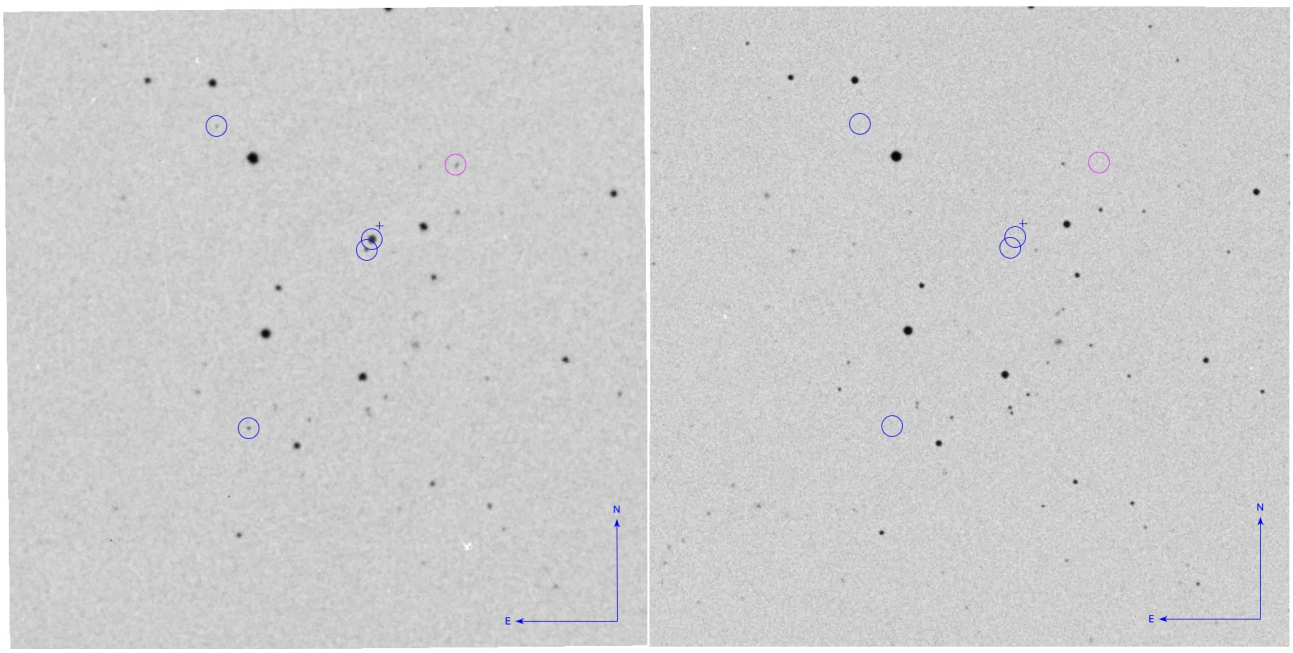

Figure 2. Candidate 2. We show the candidate in SuperCosmos scans of POSS-I red (left) and POSS-II red (right) images (inverted). Transients are marked with blue circles. The candidate with a measured coordinate is marked with a cross (+). Four transients are visible in the POSS-I image, where three follow a straight line. See Figure 7 for a version with drawn lines that shows the possible alignment. Box size is 10×10 arcmin^2.

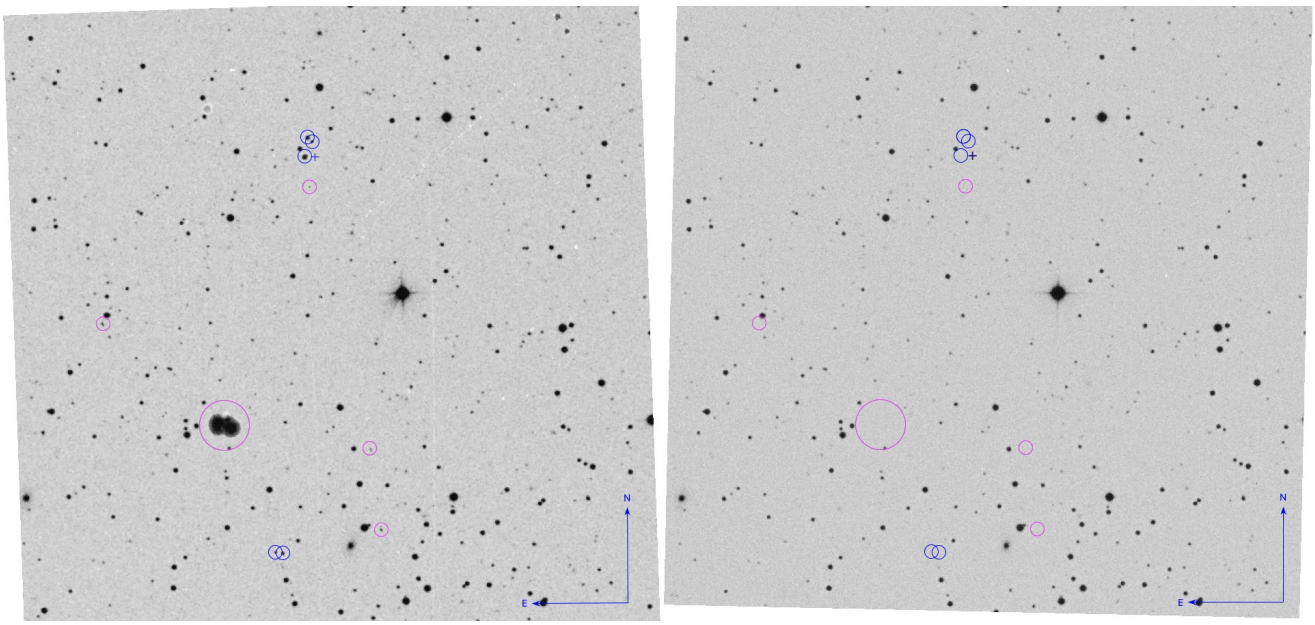

Figure 3. Candidate 3. We show the candidate in SuperCosmos scans of POSS-I red (left) and POSS-II red (right) images (inverted). Transients are marked with blue circles. The candidate with a measured coordinate is marked with a cross (+) and might be slightly dubious in shape. Pink circles show defects, both plate defects and scanning defects. See Figure 8 for a version with drawn lines that shows the possible alignment. Box size is roughly 15×15 arcmin^2.

As the area A is different for each case, we can only estimate the expected number of r-point alignments μ_r within a given field A. As suggested in Villarroel et al. (2022a), we use the generalized formula from Edmunds & George (1985),

$$\mu_r = \frac{\pi\, 2^{r-2}\, n^r\, p_{\max}^{r-2}\, A}{\Gamma(r-1)} \int_0^{d_{\max}} x^{r-1}\, e^{-2x\, n\, p_{\max}}\, dx, \qquad (1)$$

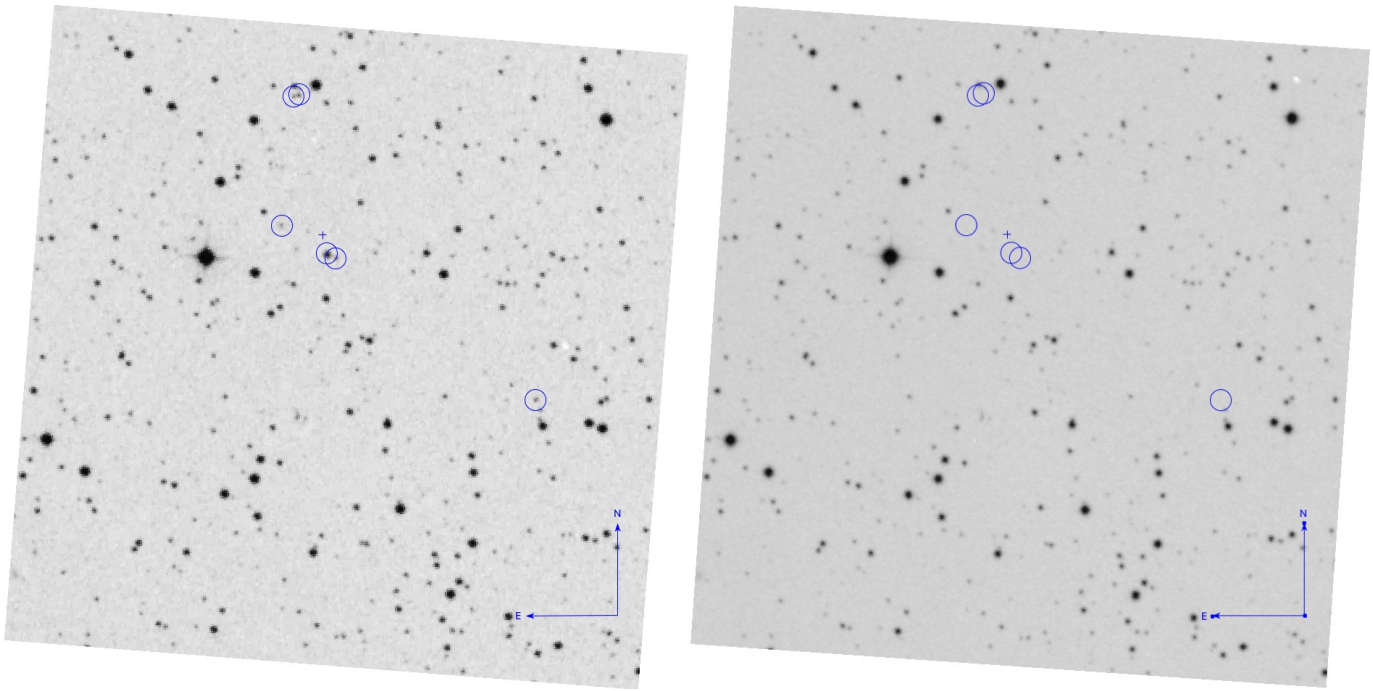

Figure 4. Candidate 4. We show the candidate in SuperCosmos scans of POSS-I red (left) and POSS-II red (right) images (inverted). Transients are marked with blue circles. The candidate with a measured coordinate is marked with a cross (+). See Figure 9 for a version with drawn lines that shows the possible alignment. Box size is 12×12 arcmin^2.

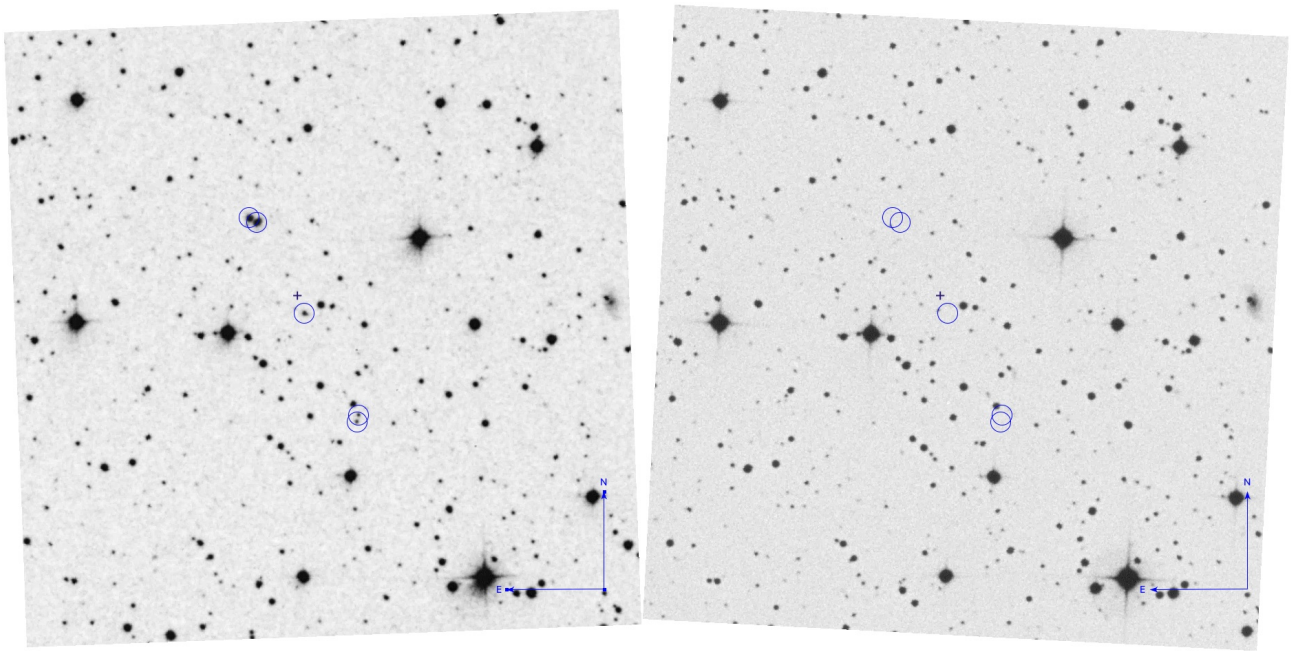

Figure 5. Candidate 5. We show the candidate in SuperCosmos scans of POSS-I red (left) and POSS-II red (right) images (inverted). Transients are marked with blue circles. The candidate with a measured coordinate is marked with a cross (+). See Figure 10 for a version with drawn lines that shows the possible alignment. Box size is 10×10 arcmin^2.

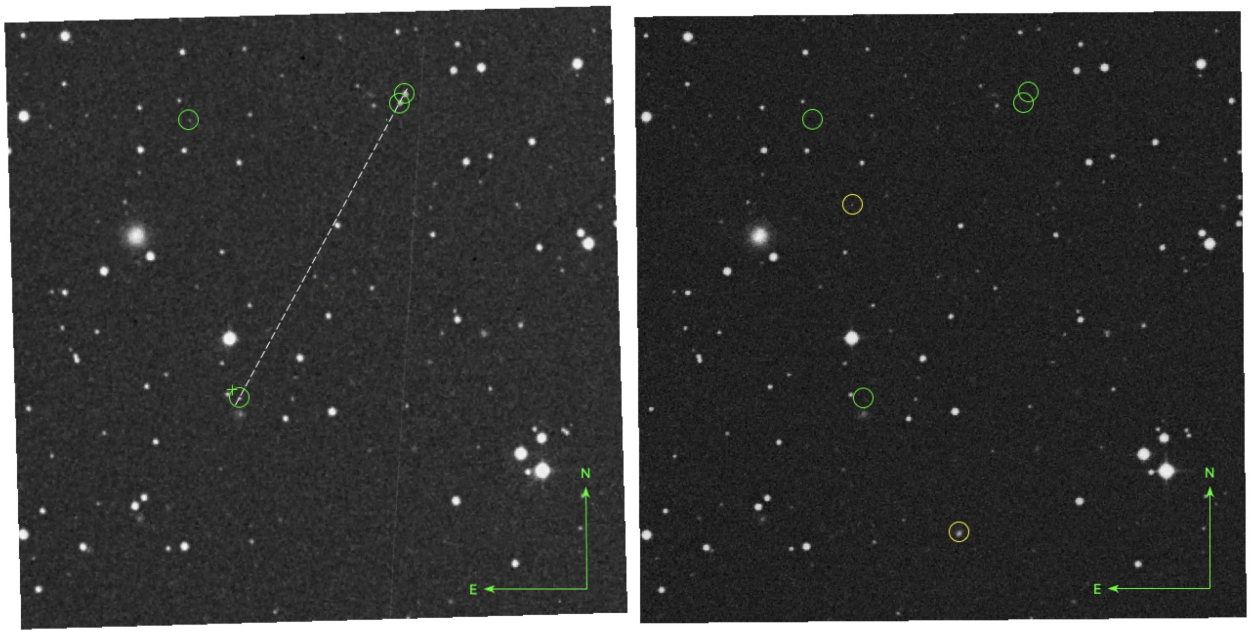

Figure 6. Candidate 1. We show the candidate in SuperCosmos scans of POSS-I red (left) and POSS-II red (right) images. Transients are marked with green circles. The candidate with a measured coordinate is marked with a cross (+). A dashed white line shows the alignment. Yellow circles show defects. Also the white line crossing the POSS-I field is a scanning defect. We see 4 transients in the POSS-I images where three follow a straight line.

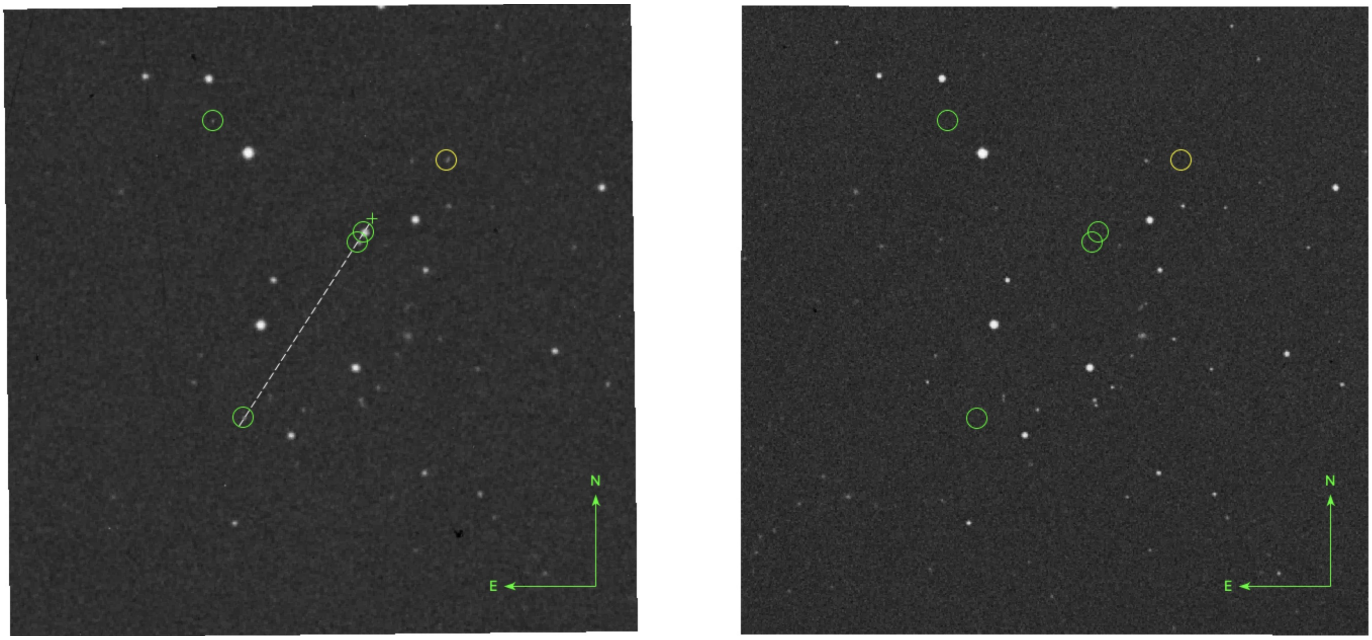

Figure 7. Candidate 2. We show the candidate in SuperCosmos scans of POSS-I red (left) and POSS-II red (right) images. Transients are marked with green circles. The candidate with a measured coordinate is marked with a cross (+). A dashed white line shows the alignment. Yellow circles show defects. Also the white line crossing the POSS-I field is a scanning defect. We see 4 transients in the POSS-I images where three follow a straight line.

where Γ is the gamma function, $n = N/A$, and all other quantities are as previously defined, with lengths given in arcmin and, consequently, the area A is in arcmin^2. As in Villarroel et al. (2022a) we use, for practical reasons, a limiting case of this generalization,

$$\mu_r \approx \frac{\pi\, 2^{r-2}\, n^r\, p_{\max}^{r-2}\, d_{\max}^r\, A}{r\,(r-2)!}, \quad r = 3, 4, 5, \cdots, \tag{2}$$

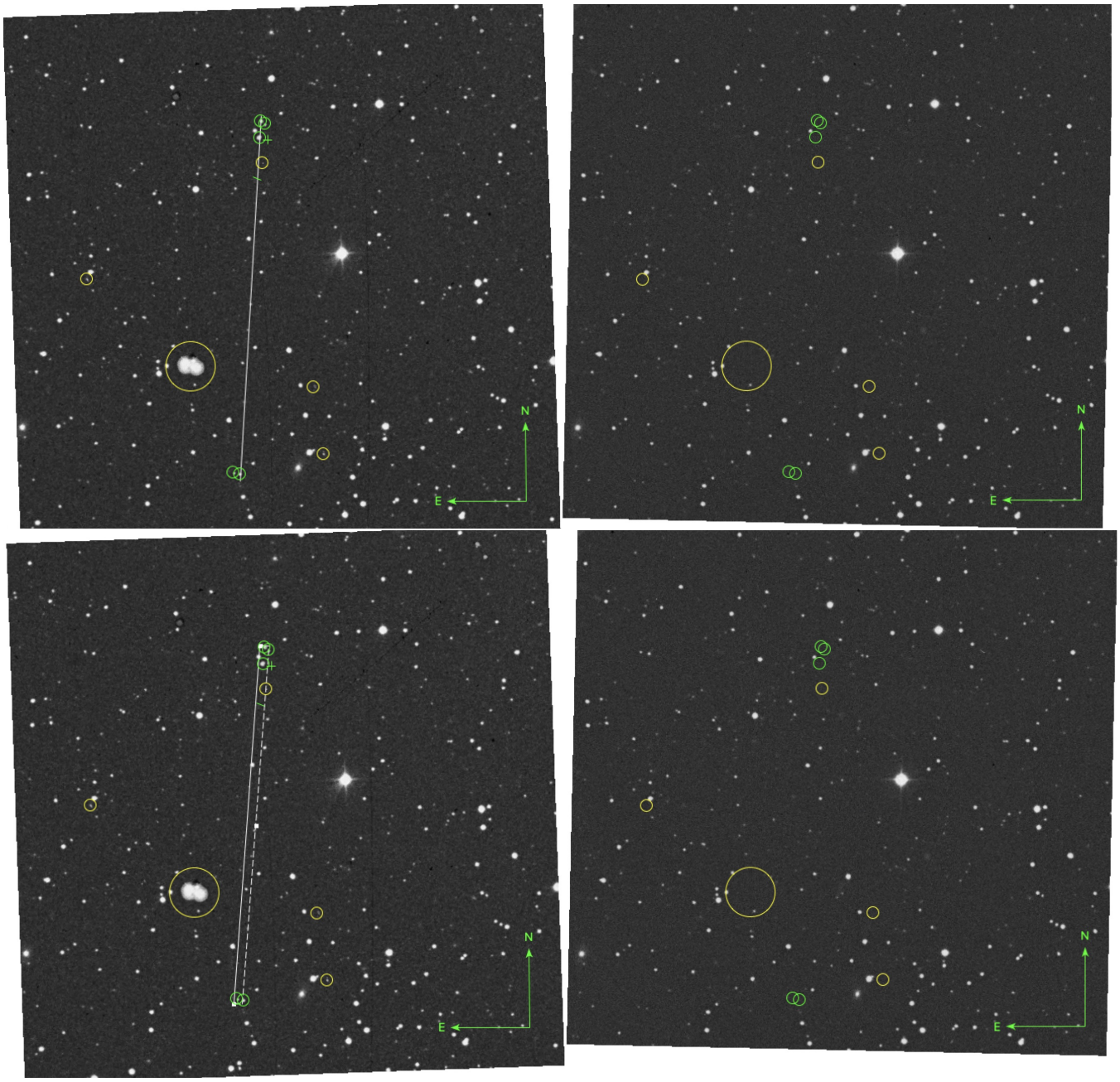

Figure 8. Candidate 3. We show the candidate in SuperCosmos scans of POSS-I red (left) and POSS-II red (right) images. The upper row shows a 3-point alignment within 1″–2″. The lower row shows a 5-point alignment of within 15″. Transients are marked with green circles. The candidate with a measured coordinate is marked with a cross (+) and might be slightly dubious in shape. The dashed lines shows the alignment (the white double line for the thicker alignment below). Yellow circles show defects, both plate defects and scanning defects.

which is a good approximation when $2\,d_{\max}\,p_{\max}\,n \ll 1$ and simplifies the calculations considerably. For the present study Equations (1) and (2) should yield very similar results, since $2\,d_{\max}\,p_{\max}\,n \lesssim 0.01$ for all cases considered.

We apply Equation (2) to calculate the expected number of r-point alignments μ_r for each case. We include all measurements in Table 2. The short list includes both 3-point alignments and 4-point alignments. Since each candidate case only has one alignment, the probability is given by the expectation value, $\mathcal{P} \sim \mu_r$. We can see that several of the cases are significantly statistically improbable (3σ–4σ) to happen in a single image.

The probability estimate is also very sensitive to the total number of transients (N) present. This number depends

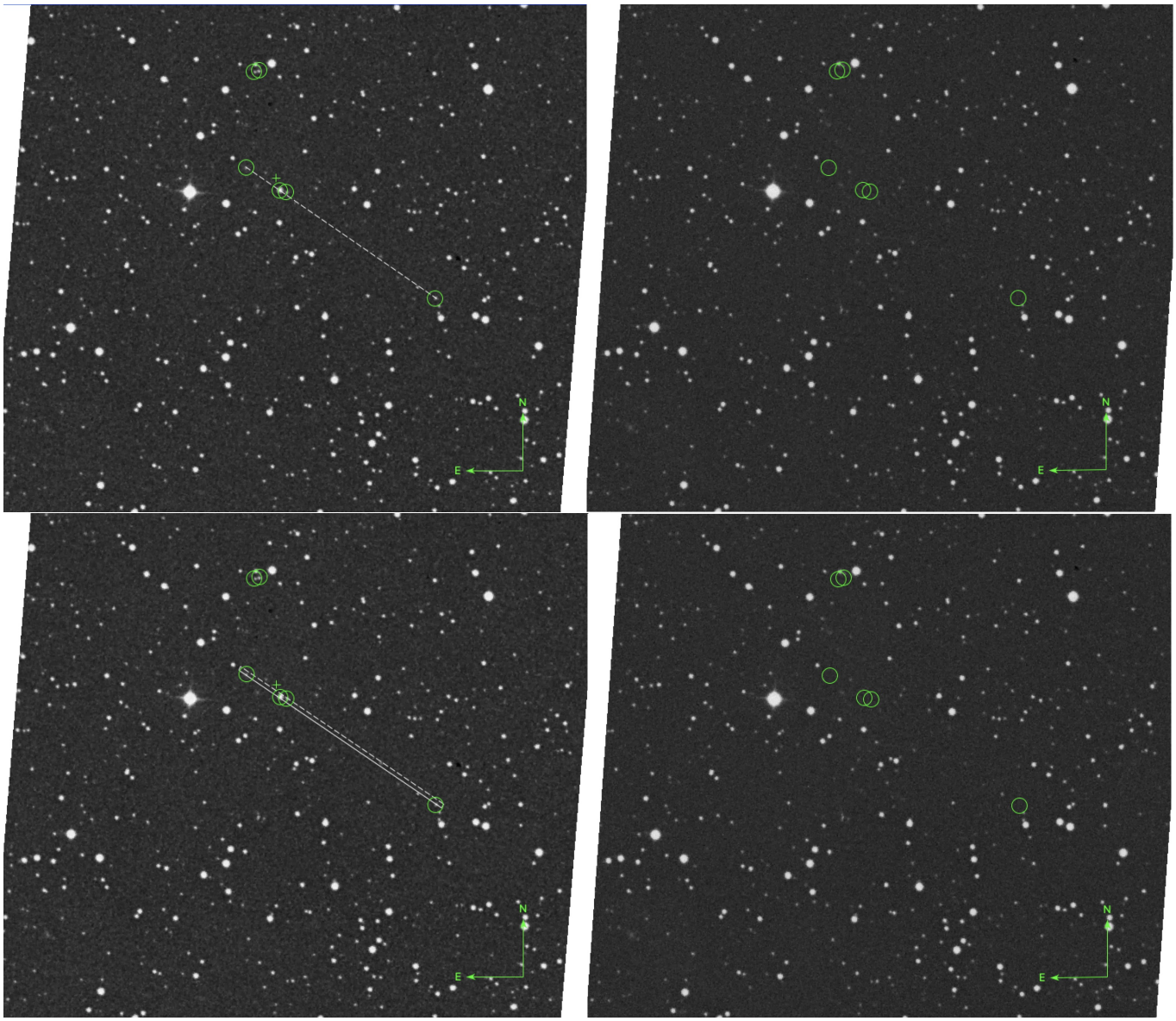

Figure 9. Candidate 4. We show the candidate in SuperCosmos scans of POSS-I red (left) and POSS-II red (right) images. The upper row shows a 3-point alignment within 1″. The lower row shows a 4-point alignment of within 5″. Transients are marked with green circles. The candidate with a measured coordinate is marked with a cross (+). The dashed lines shows the alignment (the white double line for the thicker alignment below).

strongly on the visual inspection that was made by blinking the POSS-I and POSS-II images in SAOImage DS9, taking into account the differences in depth. Any missed transients will change the value of N, and hence the estimated probability.

However, to estimate exactly the *total* probability $\mathcal{P}_{\rm tot}$ of each single event to happen during our searches, two more factors influence the total probability. The first is the probability for obtaining a perfectly 1, 2, … or N' star-like plate flaws within the same area of an image. Given the rarity of encountering a star-like plate defect, and even less so with a matching FWHM as the normal stars of the same magnitude range in the field, it may be even more unusual to encounter 2, or 3, or 4 plate flaws that all have the same coincidental features and this lowers dramatically the total probability of the event. The second factor is the total number of multiple transients in our data set: if there are sufficiently many star-like plate flaws causing "multiple transients," some of these will line up. With an infinite data set, any type of constellations will be found. This factor will, contrary to the first factor, increase the total probability for an event to occur.

Unfortunately, we have no grasp or means of estimating either of the two factors. Therefore, it is easier to examine the

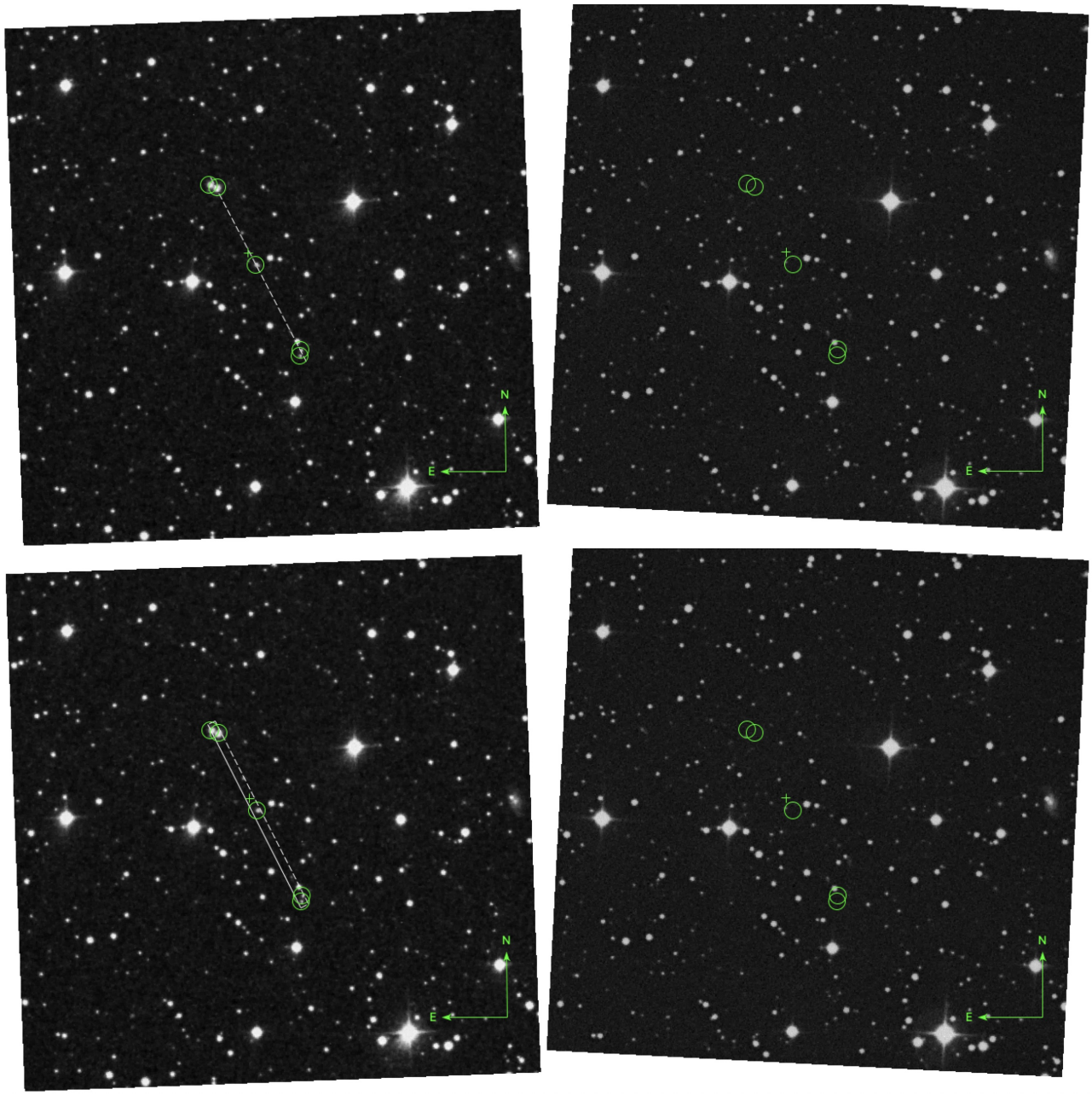

Figure 10. Candidate 5. We show the candidate in SuperCosmos scans of POSS-I red (left) and POSS-II red (right) images. The upper row shows a 3-point alignment within 1″. The lower row shows a 5-point alignment of within 10″. Transients are marked with green circles. The candidate with a measured coordinate is marked with a cross (+). The dashed lines shows the alignment (the white double line for the thicker alignment below).

effect of the choice of $p_{\max}$ on the probability estimates for single images. The choice of $p_{\max}$ depends on the science question of interest: are we interested whether the objects are truly aligned or whether they are just non-random? Showing non-randomness is all that is needed to argue for the authenticity of the points, but not necessarily enough to argue that they truly are aligned as in the case of GSO glints. We use Table 3 to adopt other values of $p_{\max}$, setting it equal to FWHM of the smallest star in an alignment (e.g., for Candidate 1, FWHM $= 2\farcs7$). Doing this, we see that all 3-point alignments are non-interesting events with $p > 0.05$ (less significant than 2σ), with an exception of the borderline case of Candidate 2. This shows that for POSS-I data where the seeing in general is rather large, 3-point alignments of simultaneous transients do not provide significant proof against randomness. The interesting cases are the 4-point and

Table 3
Measurements

Candidates 1–5					
Object	R.A.	Decl. (sexag., J2000)	FWHM (pixel)	FWHM (arcsec)	*R*
object1	2:29:37.57	+28:36:31.58	4.0	2.7	18.9
object2*	2:29:21.38	+28:36:57.89	7.2	4.8	16.6
object3*	2:29:21.76	+28:36:49.09	7.6	5.1	17.0
object4†*	2:29:33.80	+28:31:56.83	4.1	2.7	18.3
Date of observation = 1954-10-04					
Object	R.A.	Decl. (sexag., J2000)	FWHM (pixel)	FWHM (arcsec)	*R*
object1	3:05:52.34	+8:00:16.97	3.8	2.5	19.2
object2†*	3:05:42.46	+7:58:30.22	10.0	5.7	15.2
object3*	3:05:42.81	+7:58:20.56	5.9	4.0	17.9
object4*	3:05:50.24	+7:55:33.86	4.4	2.9	18.3
Date of observation = 1955-01-14					
Object	R.A.	Decl. (sexag., J2000)	FWHM (pixel)	FWHM (arcsec)	*R*
object1*	3:08:29.90	+34:31:25.73	6.2	4.2	17.1
object2*	3:08:30.72	+34:31:27.44	5.2	3.5	18.1
object3†*	3:08:27.42	+34:40:46.00	9.9	6.6	15.4
object4*	3:08:27.05	+34:41:13.49	8.1	5.4	16.1
object5*	3:08:26.56	+34:41:07.89	6.0	4.0	17.1
Date of observation = 1954-12-21					
Object	R.A.	Decl. (sexag., J2000)	FWHM (pixel)	FWHM (arcsec)	*R*
object1	21:24:45.51	+68:34:00.29	4.4	2.9	N.A.
object2	21:24:44.59	+68:34:01.20	4.6	3.1	16.6
object3*	21:24:47.62	+68:31:58.92	4.4	2.9	17.9
object4†*	21:24:39.72	+68:31:31.22	8.9	6.0	15.2
object5*	21:24:38.18	+68:31:27.97	5.0	3.4	17.2
object6*	21:24:03.94	+68:29:14.36	4.6	3.1	17.8
Date of observation = 1954-08-05					
Object	R.A.	Decl. (sexag., J2000)	FWHM (pixel)	FWHM (arcsec)	*R*
object1*	19:16:51.46	+51:30:24.51	11.0	7.4	13.2
object2*	19:16:50.64	+51:30:20.86	12.0	8.0	12.7
object3†*	19:16:45.73	+51:28:52.04	7.2	4.8	16.0
object4*	19:16:40.13	+51:27:12.85	5.0	3.4	16.3
object5*	19:16:40.27	+51:27:06.29	5.5	3.7	16.0
Date of observation = 1952-07-27					

Note. We list the astrometry-improved measurements for the objects inside the green circles in Figures 1–5. Objects that are placed inside an alignment are marked with an asteriskm ∗. The central objects presented in Table 2 are marked with a dagger (†). We show the FWHM in pixel and arcsec, based on SuperCosmos POSS-I images. The SuperCosmos resolution is $0\farcs67$ pixel^{-1}. The object have an improved astrometry with help of Terapix swarp procedure, using zero-point calculations with SDSS as a reference field. The *r* magnitudes are obtained via the photometric procedure described by B. Villarroel et al. (2025 in preparation) for DSS scanned POSS-I red plates, building on methods by Andruk et al. (1995, 2017, 2019). When an object either is too faint or two objects are too close to each other, the photometry code (that measures *R* Johnson magnitudes) fails to detect them, meaning we have no photometric information. For these cases, we mark the magnitudes as Non Available (N.A.).

5-point cases, namely Candidates 3, 4 and 5. Yet, one could argue that without an inspection with a microscope one still cannot exclude plate defects.

However, what makes the events even more interesting is that Candidate 5 occurs on the same date as one of the most famous UFO mass sightings in history—namely, the 1952 Washington UFO flap (Villarroel 2024). This could be a coincidence. We also note that Candidate 1 occurs within a day of the peak of the 1954 UFO wave. We shall discuss this further in Section 10. These additional two coincidences further motivate scrutiny of the plate defect hypothesis, especially in light of the combined statistical and contextual factors presented in this study.

7. Assessment of Conventional Explanations

The central challenge of this work lies in determining whether the transients represent authentic observations. A previous analysis of the multiple transient event in Villarroel et al. (2021) ruled out all known astrophysical origins, and most instrumental causes as well. What remains is the possibility of unknown plate contamination or emulsion defects that coincidentally resemble star-like shapes, despite their variation in brightness. While gravitational lensing by a short-lived transient passing behind an undetected supermassive black hole (SMBH) was proposed in Solano et al. (2023), such a model would require an implausibly large population of undetected SMBHs in the Milky Way to explain the broader set of events found by VASCO. The phenomenon remains unresolved—now made even more intriguing by the discovery that several events are aligned along a narrow band.

A potential concern is optical ghosts. Ghosts typically exhibit extended or clumpy morphologies and do not match stellar point spread functions (PSFs). In contrast, the transients identified in both Villarroel et al. (2021) and the current study were preselected based on their PSF-like properties (Solano et al. 2022), making classical ghosting an unlikely explanation. While most optical ghosts on POSS-I plates appear extended or irregular, one might ask whether more unusual ghosting patterns—such as point-like reflections—could in principle occur. Modern CCD-based surveys using the same telescope (e.g., ZTF, PTF) have documented rare ghost patterns that, under specific optical conditions, can mimic point sources at significant angular separations from their parent stars (Waszczak et al. 2017; Irureta-Goyena et al. 2025). A dedicated optical modeling effort would be required to fully evaluate such hypothetical scenarios, taking into account the different detector areas (CCDs versus photographic plate field sizes) and pixel scales. However, such an analysis lies beyond the scope of the present study. Instead, we compare two images of the same field taken with the same configuration, separated by only 30 minutes: the red and the blue plates for the five

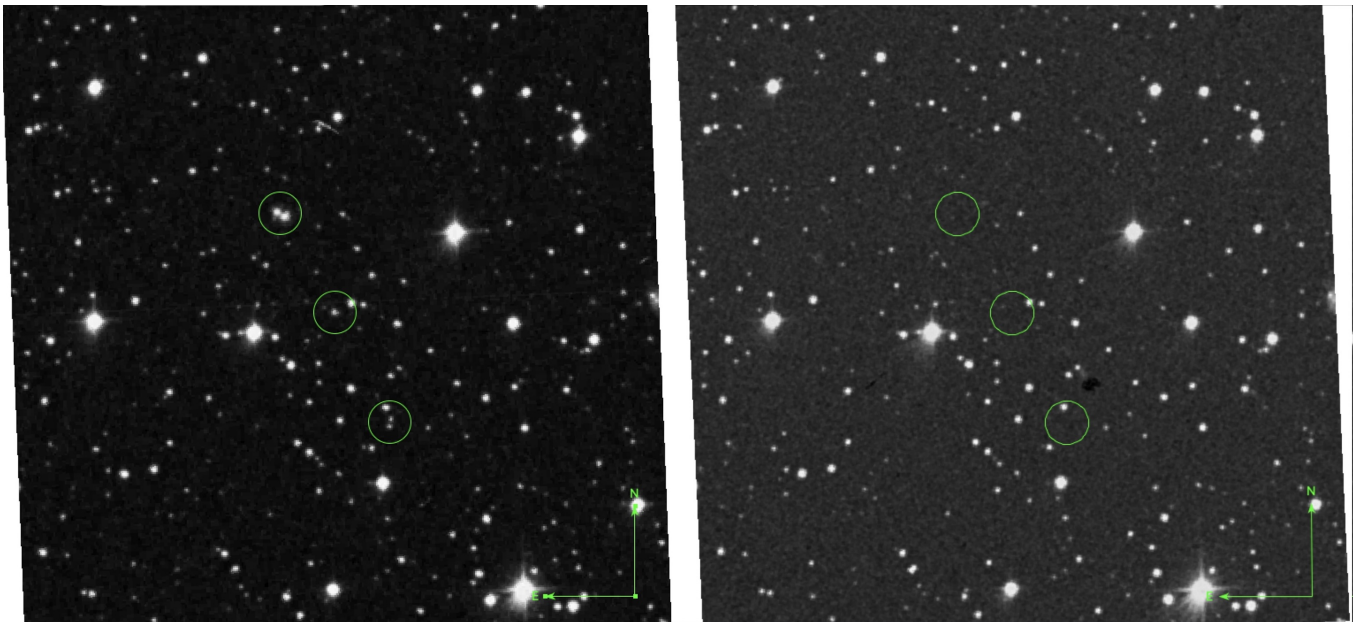

Figure 11. Red vs. blue image of Candidate 5. Comparison between the red (left) and blue (right) DSS images for Candidate 5. No coincident sources are found in the blue image.

candidates. This is similar to the case of the triple transient, where stars of about 16th magnitude appear and vanish within half an hour, yet are not seen on the corresponding blue plate with similar configuration. The blue exposures are significantly shorter, yet we do not see any similar stars or repeating patterns in them, see for example Figure 11. This further reduces the likelihood that optical ghosting can explain the alignments, though differences in exposure time and in the reflectivities of optical coatings (causing different ghosting levels in different color bands) prevents us from fully excluding it.

Another concern is photographic plate defects. Historically, astronomers have excluded single-epoch point sources to avoid false positives—an approach that also inadvertently eliminate many genuine, short-lived astronomical events. For example, Hambly & Blair (2024) argued that the transients reported in Villarroel et al. (2021), despite their point-like morphology, are likely emulsion artifacts. This conclusion was primarily based on the finding that the transients exhibit slightly narrower full width at half maximum (FWHM) values, on average, compared to normal stars. However, the analysis did not account for the known nonlinearity of photographic emulsions, which causes fainter sources to naturally exhibit narrower profiles. In addition, the "artifact" sample in their study was selected using criteria that mirror the VASCO project's transient selection pipeline, which may introduce circular reasoning. Crucially, the study did not consider that sub-second optical flashes are predicted—on physical grounds—to appear sharper and more circular than stars in long-exposure plates, due to the absence of atmospheric seeing, wind shake, and tracking-induced smearing. These effects are discussed in detail in a dedicated technical commentary (Villarroel et al. 2025a). To date, no study has systematically quantified the fraction of single-plate detections that are authentic transient phenomena versus coincidentally star-like emulsion defects.

A summary of excluded astrophysical, observational, and instrumental causes is provided in Villarroel et al. (2021). Assuming the observed transients are genuine and not artifacts, we turn to alternative physical explanations beyond the GSO glint hypothesis.

Point-like events could result from either reflected sunlight or intrinsic emission. As shown in Villarroel et al. (2021), such objects must be located within the solar system. We consider four broad possibilities: (i) the objects are inside Earth's atmosphere, (ii) they are in low Earth orbit (LEO), (iii) they are in GSO, or (iv) they are located at significantly greater distances.

If the transients originated from luminous or reflective atmospheric objects, they should leave visible trails over the 45–50 minutes POSS-I exposures, given that the telescope tracked stars during imaging. Stationary objects would also appear streaked. Objects very close to the observer would appear significantly out of focus due to proximity to the focal plane. For instance, an object at 50 km altitude would suffer a defocus of several hundred microns on the Palomar 48 inch system, resulting in an extended PSF incompatible with a stellar appearance. Only at altitudes above several hundred kilometers would point-like morphology be achievable. This effectively rules out phenomena such as red sprites or rare

luminous atmospheric events like the Hessdalen phenomenon (Teodorani 2004). The only plausible scenario in which multiple objects within Earth's atmosphere could produce point-like transients without visible trails is if they were light-emitting and appeared simultaneously for a split second—brief enough to avoid leaving motion blur—before vanishing. However, such objects within the atmosphere would be subject to focal blur. Alternatively, they would need to mimic the appearance of stars as seen from Earth. While speculative, such a scenario cannot be ruled out a priori and would fall under the category of unidentified aerial phenomena. Some asymmetries observed in, for instance, Candidate 5, might still be marginally consistent with high-altitude sources near the upper atmosphere. All plausible scenarios would fit with the observations of UAP, see Knuth et al. (2025).

LEO-based explanations are not impossible, but they are much less likely. PSF-like glints due to short millisecond flashes can be produced at any orbit altitude by rapidly spinning objects. Nevertheless, objects in LEO typically leave continuous trails, and explanations involving glints from experimental rockets or missiles at altitudes of 100–200 km are improbable due to their rapid motion and constrained illumination geometry. Further, empirical studies based on short-exposure CCD surveys (e.g., Corbett et al. 2020; Nir et al. 2021) have shown that most PSF-like glints are associated with GSO. However, if an object were capable of actively controlling both its motion and its optical signature as perceived from Earth-based observatories, then altitude constraints would no longer apply. Such a scenario would imply an engineered system of extraordinary sophistication.

We also considered more distant origins. As discussed in Villarroel et al. (2021), fast-moving Solar System objects such as asteroids will produce trails, while slow-moving ones should appear in multiple images taken close in time. Objects like tumbling interstellar bodies (e.g., *'Oumuamua*) would also produce visible trails across long exposures. Hence, no known population of solar system or interstellar objects can explain point-like transients that appear only in one long exposure and are entirely absent shortly before and after.

While we cannot exhaustively rule out all possible explanations, including those not yet imagined, the absence of known natural or instrumental causes—combined with the spatial alignment of certain events along a narrow band—calls for further investigation. And maybe the simplest way of testing the mechanism behind these flashes, is by performing a test that can reveal whether they originate from solar reflections—or if not.

8. Testing the Solar Reflection Hypothesis

The VASCO project has identified thousands of short-lived, point-like transients in pre-Sputnik photographic plates (Villarroel et al. 2020; Solano et al. 2022). The multiple transient candidates were found among this general population, with several events sharing similar timescales, morphologies, and apparent magnitudes. It is therefore reasonable to treat the multiple transients as a statistically identifiable subpopulation within this broader distribution.

One possible interpretation for transients is that they are caused by sunlight reflecting off objects with flat surfaces in GSOs, such as small rotating objects briefly glinting as they pass through a favorable viewing geometry (Villarroel et al. 2022a). If this interpretation holds, we would expect a significant deficit of such events within Earth's shadow (umbra), where sunlight cannot reach the object to produce a glint. If the transients, on the other hand, are caused by their own emission or are due to plate defects, we would expect no deficit in the number of transients within the shadow. The method of using Earth's shadow to filter out reflections is further discussed in Villarroel et al. (2025b).

While it is possible to compute the fraction of each photographic plate that lies in Earth's shadow for any given orbital altitude, not all heights are equally meaningful for our analysis. At low altitudes (e.g., below $\sim$10,000 km), Earth's shadow may cover large fractions of the plates, making any deficit or surplus hard to interpret. While plate defects do not respond to the position of Earth's shadow, the diagnostic power of this test depends on the assumption that the shadow is randomly placed with respect to plate geometry and artifact distribution. When the shadow covers a large portion of the plate (e.g., $>$50%), this assumption breaks down, and even a random distribution of artifacts will naturally yield an overdensity in the shadowed region. In such cases, the test becomes less sensitive to systematic avoidance, making small shadow coverages (e.g., $<$5%–10%) more reliable.

Moreover, reflective objects in low orbits tend to move rapidly and would often appear as streaks rather than point-spread-function (PSF)-like transients. Since our sample only includes PSF-like detections, it is physically unlikely that many of them originate from low Earth orbits, where glints would need to be extremely short-lived (on the order of milliseconds). Nir et al. (2021) show that most sub-second flares are glints of sunlight reflected from satellites in geosynchronous and graveyard orbits. For these reasons, we focus our main analysis on altitudes where less than 5% of the field is typically shadowed—regions where the shadow behaves approximately randomly, and where reflective glints, if present, would be both detectable and physically plausible.

We use the transient candidates from Solano et al. (2022), but with the additional requirement that they have no counterparts within 5″ in Gaia, Pan-STARRS and NeoWise. Furthermore, we restrict our analysis to objects in the northern hemisphere (decl. $>$ 0°). This yields a sample of 106,339 transients, which we use for our study.

An important note about the sample is that, contrary to the other transient candidates discussed throughout the paper, this

Table 4
Comparison of Earth's Umbral Shadow Coverage with Observed Transient Fractions in the Northern Celestial Hemisphere (20,626.5 square degrees)

Alt. (km)	θ (deg)	N	$A_{\rm sph}$	$A_{\rm pl}$	$f_{\rm sph}$	$f_{\rm pl}$	$f_{\rm obs}$	$f_{\rm sph}/f_{\rm obs}$
42,164	8.69	349	237.4	237.2	0.0115	0.0115	0.00328	3.50
80,000	4.57	79	66.0	65.6	0.0032	0.0032	0.00074	4.32

Note. We show the altitude (km), the shadow radius in degrees (θ), the number N of VASCO transients detected inside the shadow, the shadow area $A_{\rm sph}$ assuming spherical sky geometry (sq. deg), shadow area $A_{\rm pl}$ assuming planar approximation (sq. deg), expected fraction $f_{\rm sph}$ of transients in shadow using spherical area, expected fraction $f_{\rm pl}$ using planar area, the observed fraction $f_{\rm obs}$ of VASCO transients in shadow, and the ratio $f_{\rm sph}/f_{\rm obs}$.

sample has not been visually inspected. As such, it is expected to contain a substantial number of false positives, including clustered artifacts such as edge fingerprints or other plate defects that contaminate our sample. In addition, the spatial distribution of the sample is not isotropic due to inhomogeneous sky coverage in the original POSS-1 survey. Some regions of the sky are more densely sampled than others, leading to variation in the overall detection density.

However, these effects do not bias the results of our shadow analysis. The reason is that we are comparing a small, well-defined subset of this population—those that fall within the Earth's shadow cone at the time of observation—with the rest of the same population. Since the selection effects and potential false positives affect both the shadowed and unshadowed regions similarly, any large and statistically significant difference in detection rates between these regions must reflect an intrinsic property of the detections themselves, not an observational bias. Or to express it simply: plate defects do not know where the Earth's shadow is, and have no reason to avoid that region more than any other.

The fraction of transients expected within the umbra depends on the angular radius of Earth's shadow at different altitudes. We use the software library `earthshadow` published by Guy Nir published (Guy Nir's code 2024) to estimate the size of the Earth's Shadow at 40,000 km ($8\overset{\circ}{.}69$) and 80,000 km ($4\overset{\circ}{.}57$). The code determines whether a given point at a specified altitude and geographic position lies inside Earth's shadow, based on the solar angle and the geometric configuration of the Sun, Earth, and the object. We apply it to each transient using their J2000 coordinates and Julian Dates. We compare the expected and observed rates for two different altitudes capable of producing PSF-like transients, namely 42,164 km and 80,000 km. We can calculate the expectations based on how large fraction of the northern hemisphere is covered by the shadow, and compare with the observed fractions. We calculate the area in two different ways, both based on based on spherical geometry: $2\pi(1-\cos\theta)$) as well as planar sky coverage, as an approximation. Table 4 shows the results. We note that multiple plates ($\sim$10) fall within Earth's shadow, so the observed deficit is not driven by a single outlier plate.

To estimate the statistical significance of the difference in transient detection rates within Earth's umbra at different altitudes, we compute Poisson uncertainties for the observed and expected fractions. At 42,164 km altitude, we expect $N = 1223$ transients in shadow out of 106,339 total, corresponding to an expected fraction of $f_{\rm exp}$=0.0115 $\pm$ 0.00033. However, we observe only $N = 349$ transients in shadow, yielding $f_{\rm obs} = 0.00328 \pm 0.00018$. The difference between these fractions is highly significant, with a significance level of 21.9σ, computed by combining the Poisson uncertainties in quadrature:

$$\sigma = \frac{|f_{\rm exp} - f_{\rm obs}|}{\sqrt{\sigma_{\rm exp}^2 + \sigma_{\rm obs}^2}} = \frac{|0.0115 - 0.00328|}{\sqrt{(0.00033)^2 + (0.00018)^2}} \approx 21.9.$$

At 80,000 km altitude, we expect $N = 339$ transients in shadow out of 106,339 total, corresponding to a fraction of $f_{\rm exp}$=0.00319 $\pm$ 0.00017. However, we find only $N = 79$ transients in shadow, yielding $f_{\rm obs} = 0.00074 \pm 0.000084$. The difference in these observed fractions is also highly significant, with a significance level of 12.7σ, computed by combining the Poisson uncertainties in quadrature:

$$\sigma = \frac{|f_{\rm exp} - f_{\rm obs}|}{\sqrt{\sigma_{\rm exp}^2 + \sigma_{\rm obs}^2}} = \frac{|0.00319 - 0.00074|}{\sqrt{(0.00017)^2 + (0.000084)^2}} \approx 12.7.$$

This result further strengthens the conclusion that sunlight is necessary for producing the transient events. The strong deficit of transients within the Earth's umbra suggests that the majority of these events depend on sunlight illumination, consistent with the glint hypothesis. This strongly defies the plate defect hypothesis and many of the alternative hypotheses presented in Section 7.

We performed an additional test to estimate the actual fraction of the survey sky that was covered by Earth's shadow during the actual POSS-I observations, and to compare it to the

actual observed fraction of transients falling within the shadow. The transient sample is based on 635 unique photographic plates, each with a designated central coordinate (R.A., decl.) in J2000 and a corresponding observation time. Each plate spans $6^\circ \times 6^\circ$ on the sky, as listed by STScI. We simulated 180 random points per plate, for a total of 114,300 points. For each simulated point, we tested whether it would fall within Earth's shadow at a geosynchronous altitude (42,164 km) during a 50 minutes exposure starting from the recorded observation.

Out of the 114,300 simulated points (180 points per plate), 610 were found to lie within Earth's shadow, implying that approximately 0.53% of the survey area should be shadowed at GSO. However, in our actual transient data set, only 349/107,875, 0.32% of the events occur within the shadow, corresponding to a $\sim$39% deficit, significant at the 7.6σ level. We repeated the same procedure at a higher altitude of 80,000 km. In this case, the actual shadow coverage drops to (109/114,300) 0.1%, while the observed fraction of transients (76/107,875) within the shadow is only 0.07%—a $\sim$26% deficit, significant at the 2σ level. The simulated points within each plate are used solely to estimate the expected geometric coverage of the Earth's shadow during the exposure time, and are not meant to represent the spatial distribution of actual transients. This also suggests that a larger fraction of objects may be located near GSO than at 80,000 km, although the limited number of events at 80,000 km makes the comparison statistically uncertain.

We perform an additional, conservative test on the transients, this time assuming a total exposure time of 50 minutes. While our main shadow test assumes that the transient event occurs at a single moment (which is reasonable given their short duration), we now test whether the Earth's shadow passes through the transient's position at *any time* during a 50 minutes window. This increases the chance that the transient would fall within the shadow. We find that 387 (0.3587%) are in the Earth Shadow at 42,168 km, and 80 (0.072%) at 80,000 km. Even under this generous upper limit assumption, where a transient is considered shadowed if the Earth's shadow passes through its position at *any* during a 50 minutes exposure, the deficit remains strong. This result provides robust evidence that the VASCO transients systematically avoid Earth's shadow, consistent with a population of reflective objects that are only visible while sunlit.

The normalization technique presented here is grounded in a direct simulation of shadow coverage based on the actual photographic plates used in the survey. Each plate's position and observation were used to simulate uniformly distributed test points across the plate area, allowing us to empirically estimate the expected fraction of the survey sky that falls within Earth's shadow. This approach minimizes assumptions and avoids potential systematic biases that may arise from analytical solid angle approximations. To avoid introducing spatial selection bias, we include all observed transients in the analysis, including those clustered near the edges of the plates, since plate defects do not know where is the Earth's shadow. As a quick check, nevertheless, we also test by masking edge transients ($>2^\circ$ from plate center) to remove all artifacts close to the plate edge. Removing the edge of the plate in the analysis, yields a similar $\sim$30% deficit in Earth's shadow, though with borderline significance (2.6σ) due to the decrease in sample sizes.

As a note, at low altitudes—where the shadow covers a large fraction of the plate—it is also possible to observe a significant overdensity of transients in the shadowed region. This is a natural consequence of the geometric coverage: when most of the field lies in shadow, any transient—regardless of origin—is statistically more likely to fall there. Such overdensities are therefore not physically meaningful and cannot be used to infer the nature or altitude of the objects. We therefore recommend restricting the analysis to altitudes where the Earth's shadow covers no more than 5% of the plate area, in order to preserve the assumption that its placement is effectively random with respect to plate geometry and defect distribution.

An important implication of this analysis is that the total number of glinting objects near GSO may be significantly underestimated if one only considers the aligned transient candidates, since they represent only a minor subset (albeit visually vetted) of the full transient population. Our results suggest that a much larger population of objects capable of producing sunlight reflections exists, as inferred from the full VASCO transient sample. This systematic deficit of transients in Earth's shadow—especially at altitudes where sunlight reflections dominate—supports the interpretation that a significant fraction, roughly $\sim$1/3rd of all VASCO transients, are caused by highly reflective objects in GSO. However, in order to determine the absolute number of such objects, we would need to quantify the true fraction of false positives in the sample—such as artifacts and plate defects—a major undertaking that will be addressed in a forthcoming study.

9. The GSO Hypothesis

9.1. Object Properties

In this section, we discuss the conditions under which reflections from objects in GSO could produce the observed glints.

An important question is what types of object shapes and reflective geometries are capable of creating the transient signatures observed in the POSS-I plates. A rapidly spinning object may produce multiple glints during a 50 minutes exposure, whereas a more slowly rotating object might generate only one or two.

If we assume a fast spin rated interpret the observed stripe length $d_{\max}$ as corresponding to the path traversed by the

object during the exposure, we can estimate a projected velocity of approximately $0\farcs5\ s^{-1}$. This is significantly slower than the nominal angular velocity of an object at GSO ($\sim 15''\ s^{-1}$). Under these circumstances, we might expect additional transients to be visible along the same narrow band, particularly if the image were extended. Conversely, if the object spins slowly and has only a few small, highly reflective surfaces distributed across a predominantly non-reflective structure, glints may occur only briefly during the exposure, and only at specific orientations.

To explore this further, we use the open-source graphics engine *Blender*[22] to simulate how various 3D shapes could produce glinting patterns similar to those observed. We model five distinct geometries: a sphere, a multi-faceted polyhedron, a cone, a double pyramid, and a structure with two reflective panels. Each shape is composed primarily of non-reflective material, with limited flat surfaces capable of producing strong specular reflections when oriented precisely between the observer and the Sun. In addition to rotation, we allow for precession in some models, which modulates the visibility and timing of glints. The five test geometries are shown in Figure 12.

As expected, a purely spherical object does not generate short, distinct glints; flat, mirror-like surfaces are required. In the cone model, we assume that that the top and bottom surfaces are reflective, yielding double glints per rotation cycle. Adding precession further restricts glint visibility, producing only a few observable flashes per exposure.

The double pyramid model illustrates another plausible case: a reflective structure that becomes partially degraded over time, leaving only small reflective regions. With rotation and precession, such objects may produce intermittent glints, consistent with what we observe in the data.

Overall, we find that each of the five test shapes—under specific assumptions regarding spin, precession, and reflective surface coverage—can, in principle, reproduce a glinting pattern compatible with the transients observed in POSS-I images.

The geometric models presented in this section are intended to demonstrate the plausibility of producing aligned glint patterns from tumbling or precessing objects in high-altitude orbits. We emphasize that these models are illustrative rather than predictive, and no attempt is made to fit the specific time separations or angular offsets of the individual candidates.

While no clear periodicity has been identified in the current POSS-I data, it is well known from modern short-exposure surveys that some Earth-orbiting objects, including those in GSO, can produce isolated, PSF-like glints without clear repetition patterns (e.g., Nir et al. 2021). This lack of periodicity may result from slow rotation, irregular shapes, or specific phase-angle constraints that produce only a few observable flashes per orbital cycle.

Additionally, the observed sky distribution of aligned transients does not always follow a simple great-circle geometry, which could reflect the possibility of complex trajectories, attitude drift, or even the presence of multiple independent objects. Powered objects could even change their altitudes or trajectories. We acknowledge these uncertainties and note that more detailed modeling would be required to establish stronger constraints on orbital parameters or glint periodicity.

9.2. The Background Density

We use the 106,339 transients with decl. $> 0°$ to estimate a rough detection rate. We also count the transients within 2° from the center to avoid potential defects on the edge of the plate (22,314 transients). About 635 plates with 50 minutes exposures on average, correspond to 529 hr and an average transient rate of 36.3 transients per plate circle of 2° radius. Based on the deficit in the Earth Shadow test in Section 8, roughly 1/3rd of the transients appear to be due to solar reflections, so roughly 12.1 transients per plate. We can simply normalize 12.1 over the exposure time and plate coverage (12.57 sq.deg), which gives us $\sim$1.1 transients hr^{-1} deg^{-2} of flux-diluted flashes, visible down to $r \sim 20$ mag. This transient rate is the sum of transients on all altitudes and distances from Earth.

Nevertheless, this comparison should be viewed as an approximate, order-of-magnitude contrast as the the number of transients per plate is very approximate. Also, modern short-exposure surveys such as ZTF operate under vastly different conditions—using CCDs, automated pipelines, and millisecond-level time resolution—whereas the POSS-I transients were recorded on photographic plates with long integration times and are subject to different detection biases and false positive rates. A rigorous comparison would require modeling of completeness, instrument sensitivity, and event classification criteria, which is beyond the scope of this study.

We can also calculate the actual number density of objects. If we assume that the population of objects has a uniform number per surface unit (n), then the number of objects (N) detectable at any given time is given by:

$$N = n \times S, \tag{3}$$

where S is the spherical survey surface containing the observed reflective objects:

$$n = \frac{N}{S}, \tag{4}$$

[22] www.blender.org

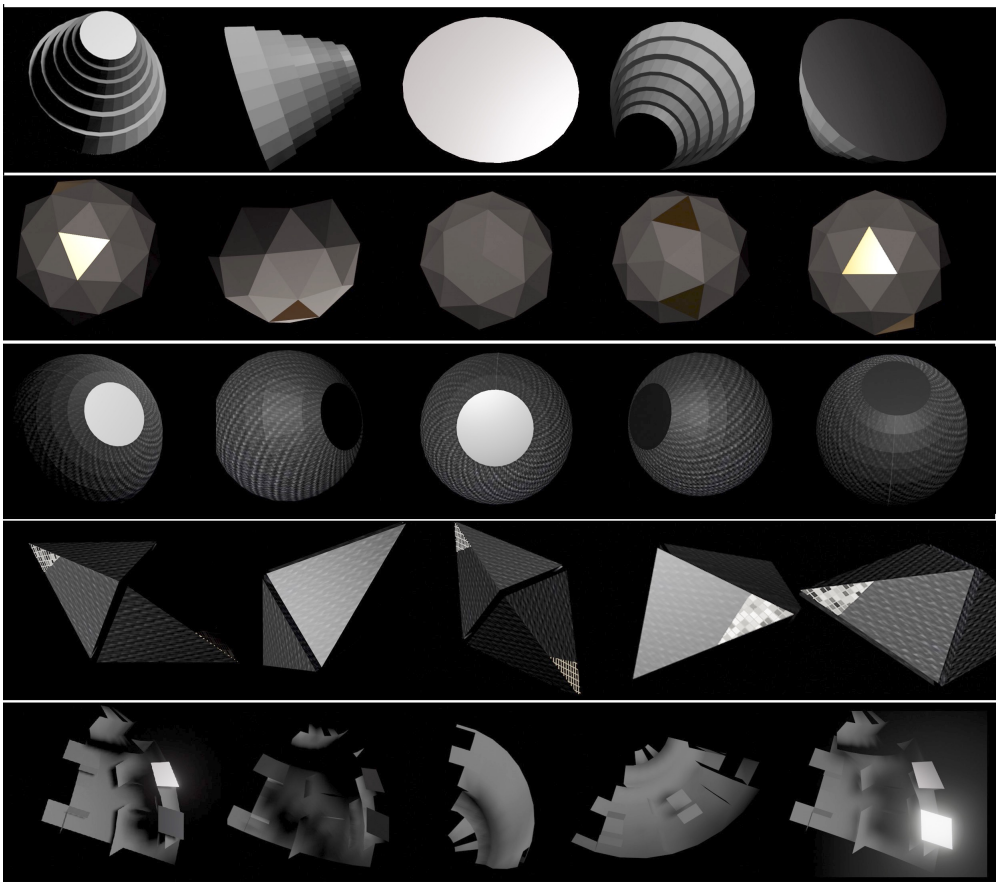

Figure 12. Simulated shapes. We show five different shapes that under slow spinning could produce a handful of glints and in particular double glints. Each shape has two highly reflective surfaces. From top to bottom: (a) cone-like shape, (b) multifaces shape, (c) sphere, (d) 3D hexagone, (e) piece of debris. Each object has both dull and reflective materials on its surface, painted in gray respective light tones. Each object spins around an axis that also has precession, causing the reflective surface not to be visible at all times.

and the surface area $S = 2\pi d^2$ is calculated for the sunlit hemisphere at the radius of a GSO d. Thus:

$$n = \frac{N}{2\pi d^2}. \tag{5}$$

We set $d = 42{,}164$ km as the radius of the GSO.

Using the glint detection rate of approximately $\sim$1.1 transients per hour per square degree (assuming one detectable glint per object per hour):

$$n_{\rm all} \approx 2.0 \times 10^{-6}\,{\rm km}^{-2}. \tag{6}$$

These estimates provide a guide to the surface number density of objects. However, not every object will produce several glints. Since some objects might produce more than one glint (see Section 3.4 in Nir et al. 2021), we can assume that one object might produce from 5 to 20 glints. The shape and the reflectivity of an object will determine the likelihood for one or more glints. This uncertainty also leads to an underestimation of the number density of objects, which could actually be even one order of magnitude higher. The surface density constraint quoted here is a first-order estimate based on our event detection rate and assumed sky coverage. These estimates do not include a full treatment of incompleteness, observational bias, or formal statistical confidence levels, and should therefore be interpreted as an indicative upper bound rather than a rigorous limit. Moreover, the true fraction of false positives in the larger sample from Solano et al. (2022), due to plate defects or other instrumental artifacts, remains unknown. While the overall statistical test in Section 8 is robust to this uncertainty, the absolute number density $n_{\rm all}$ inferred here should be interpreted with caution until a full validation of the sample has been performed.

10. Discussion

Are there signatures of artificial objects in Earth's orbit in pre-Sputnik images? This is the central question explored in the present study. We adopt a straightforward strategy: searching for multiple transients aligned along a narrow band within long-exposure photographic plates from a period prior

to known artificial satellite activity. This approach follows the principle of seeking NTAs via distinctive, low-probability observational signatures, or "smoking gun indicators" (Villarroel et al. 2021). Using the published catalog of VASCO transients in the northern hemisphere (Solano et al. 2022), we identify ∼83 initial candidate *r*-point alignments, along with a larger number of double and triple transient groupings. Triplets are of particular interest, as they are consistent with reflections from flat, rotating surfaces (Deil et al. 2009). One such example was previously reported in Solano et al. (2023).

We manually inspect all 22 candidate alignments containing four or more transients (noting that some reduce to three after closer analysis), and highlight the five most statistically significant cases in Section 6. Although the uncertainties do not allow us to compute a total occurrence probability for such alignments across the entire survey, we do estimate the chance probability of each event within a single image field. These estimates—dependent on assumptions about point-spread function widths—yield significance levels ranging from 2.5σ to 4σ for the most promising cases. Notably, three candidates with four or more aligned points emerge as especially strong, although two of them show minor morphological irregularities. These are not related to FWHM differences, which are addressed separately in the literature (Villarroel et al. 2025a). While we cannot fully exclude the possibility of rare PSF-like optical ghosts producing the alignments, we note that no similar features appear on the blue plates taken with similar configurations.

Among the remaining 3-point alignments (61 in total), some may also merit follow-up if confirmed as genuine transients. Traditionally, this would require microscopic examination of the original plates. However, our discovery of a statistically significant ($>3\sigma$) temporal correlation between VASCO transients and independent historical reports of UAPs (Bruehl & Villarroel 2025) offers additional support for the authenticity of the transients. Plate defects or scanning artifacts are expected to occur randomly in time; the fact that these transient alignments appear preferentially within a day of reported UAP events strongly disfavors instrumental or spurious origins. In this light, the correlation itself provides indirect but meaningful validation of the transients' reality—thus reducing the necessity of microscopic inspection as the only path to confirmation.

But most importantly, Section 8 presents a critical test of the glint interpretation: we find a strong deficit of transient detections, at the $\sim 22\sigma$ statistical significance level, within the Earth's umbral shadow. This is consistent with the idea that sunlight is required to produce the observed flashes. If these events are sunlight reflections off orbiting objects, they should vanish in the shadow cone of the Earth—exactly what we observe. This lends substantial support to the interpretation that the transients are real astrophysical or near-Earth events, and not plate defects or optical ghosts. The disappearance of the population in Earth's shadow would not be expected for emulsion flaws or chemical irregularities. The same holds true for optical ghosts.

Of particular interest is Candidate 5, which occurred on 1952 July 27—the second weekend of the widely documented Washington D.C. "UFO flap." This wave of sightings involved numerous radar detections and pilot observations over two consecutive weekends, July 18–19 and 26–27. Coincidentally, Candidate 1 also occurred within one day of the peak of the 1954 UFO wave. The triple transient reported in Solano et al. (2023) falls on the first weekend of the Washington event. Importantly, these candidates were analyzed before the authors became aware of their proximity to UAP reports, helping to minimize cognitive bias.

Additionally, a correlation has been found between VASCO transients and historical nuclear test dates (Bruehl & Villarroel 2025), echoing past statistical studies linking nuclear activity to increased UAP reports, see e.g., review by Knuth et al. (2025). While causality remains undetermined, the convergence of these independent correlations suggests that the VASCO transients are not random artifacts, but potentially linked to physical phenomena worthy of further investigation.

Using the theoretical framework outlined earlier, we simulate glinting patterns from plausible object shapes in GSO. These include multifaceted and partially reflective objects with slow spins and precessing axes. The inferred surface density of detectable objects is 2.0×10^{-6} km^{-2}, though this estimate is subject to uncertainty both from unknown shape and reflectivity factors (which may cause underestimation), and from the unknown fraction of false positives in the sample (which may cause overestimation). It is worth considering whether such a population could be associated with the so-called uncorrelated targets (UCTs), which have been consistently reported in substantial numbers by military optical sensors and radars since the early 1960s.[23]

Although the GSO hypothesis is consistent with the data, no clear evidence for periodic or quasi-periodic glinting has yet been identified. Objects spinning slowly or possessing complex reflective geometries may produce only a few flashes, complicating efforts to establish a repeating signature. Moreover, it remains possible that some events extend beyond the field of view of a single plate. An object moving at $\sim 10''$ per second could traverse up to 10° during a 50 minutes exposure, suggesting the possibility of longer alignment chains than those captured here.

Conversely, if all transients were to be confirmed as false positives—e.g., due to rare but star-like photographic plate artifacts—our search still constitutes a meaningful upper limit

[23] For example, see declassified U.S. Department of Defense documents released under FOIA, available via The Black Vault: https://documents2.theblackvault.com/documents/dtic/FOIA2014-128-GC8000301.pdf.

on the density of NTAs in the near-Earth environment. In this scenario, we derive a rough surface density constraint of $<10^{-6}$ objects km^{-2} for high-altitude orbits in the Earth's vicinity (thousands to hundreds of thousands of kilometers), even if this limit must be carefully approached due to the lack of modeling for bias and incompleteness. Thus, regardless of interpretation, our findings provide new constraints on possible technosignatures near Earth.

Future work should consider searching for "dashed-line" alignments over larger plate regions, and investigating subtle elongation effects in high-resolution digitizations. Such elongations could indicate motion across the sky or large object size, especially if consistent with the alignment direction.

In summary, we have presented a small but compelling set of aligned transient candidates from a pre-satellite era sky survey. While the ultimate explanation remains uncertain, the convergence of spatial alignment, statistical significance, and temporal correlation with independent aerial anomaly reports supports the view that these events are likely real—and may represent a class of astronomical phenomena not yet understood. Alternative explanations are discussed in Section 7.

11. Conclusions

This paper presents a first systematic search for multiple, simultaneously appearing and vanishing optical point sources on long-exposure photographic plates that also exhibit spatial alignment. We focus on the red POSS-I plates, and present five top candidate events with three or more transients aligned along a narrow band. The most statistically significant case (Candidate 5) coincides in time with the well-documented Washington D.C. 1952 UFO flap—one of the most prominent mass sightings of UAPs in recorded history. A separate study (Bruehl & Villarroel 2025) confirms a statistically significant ($>3\sigma$) temporal correlation between VASCO transients and independent historical UAP reports.

The origin of the transients remains unknown. One plausible explanation is that they are caused by brief light emissions from artificial objects in orbit or by objects with anomalous movements in Earth's atmosphere—emissions so brief that they appear as point sources rather than streaks, despite the telescope tracking the stars. Alternatively, they could arise from solar reflections off flat, highly reflective surfaces at geosynchronous altitudes. The latter interpretation is further supported by our shadow test in Section 8, which reveals a significant deficit of such events within the Earth's umbra, consistent with a solar reflection origin and difficult to reconcile with many explanations, including photographic plate defects.

Our results motivate continued investigation of historical sky surveys and the application of similar alignment-based detection methods to modern deep-sky imaging. Whether or not these events ultimately point to the existence of NTAs, the identification of statistically improbable, spatially aligned transients in pre-satellite data represents a novel observational anomaly deserving of further scientific attention. Future work may help clarify whether these transients constitute a new class of astronomical phenomena—or represent the first hints of artificial activity near our planet.

Acknowledgments

B.V. wishes to thank the anonymous referee, that gave challenges and suggestions that great improved this work. B.V. wishes to thank Dennis Åsberg for his support and for inspiring discussions about the work. She also wishes to thank Dave Altman for teaching her about the Washington 1952 UFO flap. B.V. also wishes to thank Geoff Marcy, Avi Loeb (Galileo project), Robert Powell (SCU/Galileo), Sarah Little (SCU/Galileo) for helpful and constructive comments.

The Digitized Sky Surveys were produced at the Space Telescope Science Institute under U.S. Government grant No. NAG W-2166. The images of these surveys are based on photographic data obtained using the Oschin Schmidt Telescope on Palomar Mountain and the UK Schmidt Telescope. The plates were processed into the present compressed digital form with the permission of these institutions. The National Geographic Society—Palomar Observatory Sky Atlas (POSS-I) was made by the California Institute of Technology with grants from the National Geographic Society. The Second Palomar Observatory Sky Survey (POSS-II) was made by the California Institute of Technology with funds from the National Science Foundation, the National Geographic Society, the Sloan Foundation, the Samuel Oschin Foundation, and the Eastman Kodak Corporation. The Oschin Schmidt Telescope is operated by the California Institute of Technology and Palomar Observatory. The UK Schmidt Telescope was operated by the Royal Observatory Edinburgh, with funding from the UK Science and Engineering Research Council (later the UK Particle Physics and Astronomy Research Council), until 1988 June, and thereafter by the Anglo-Australian Observatory. The blue plates of the southern Sky Atlas and its Equatorial Extension (together known as the SERC-J), as well as the Equatorial Red (ER), and the Second Epoch [red] Survey (SES) were all taken with the UK Schmidt. All data are subject to the copyright given in the copyright summary. Copyright information specific to individual plates is provided in the downloaded FITS headers. Supplemental funding for sky-survey work at the STScI is provided by the European Southern Observatory.

This research has made use of the Spanish Virtual Observatory (http://svo.cab.inta-csic.es) supported from Ministerio de Ciencia e Innovación through grant PID2020-112949GB-I00. B.V. is funded by the Swedish Research Council (Vetenskapsrådet, grant No. 2024-04708) and is also

supported by an anonymous donor to whom she is deeply grateful. M.E.S. acknowledges financial support from the Annie Jump Cannon Fellowship, supported by the University of Delaware and endowed by the Mount Cuba Astronomical Observatory.

Data Availability

Data will be shared on reasonable request to the corresponding author.

ORCID iDs

Alina Streblyanska https://orcid.org/0000-0001-8876-9102

References

Andruk, V., Eglitis, I., Protsyuk, Y., et al. 2019, OAP, 32, 181
Andruk, V., Kharchenko, N., Schilbach, E., & Scholz, R.-D. 1995, AN, 316, 225
Andruk, V. M., Pakuliak, L. K., Golovnia, V. V., et al. 2017, SciIn, 13, 17
Bracewell, R. N. 1960, Natur, 186, 670
Bruehl, S., & Villarroel, B. 2025, Scientific Reports, in press, https://www.researchsquare.com/article/rs-6347224/v1
Corbett, H., Law, N. M., Soto, A. V., et al. 2020, ApJL, 903, L27
Deil, C., Domainko, W., Hermann, G., et al. 2009, APh, 31, 156
Edmunds, M. G. 1981, Natur, 290, 481
Edmunds, M. G., & George, G. H. 1985, MNRAS, 213, 905
Freitas, R. A., Jr., & Valdes, F. 1980, Icar, 42, 442
Freitas, R. A., Jr., & Valdes, F. 1985, AcAau, 12, 1027
Greiner, J., Wenzel, W., & Degel, J. 1990, A&A, 234, 251
Grindlay, J., Tang, S., Los, E., & Servillat, M. 2012, in IAU Symp. 285, New Horizons in Time-Domain Astronomy, Proc. Int. Astronomical Union (Cambridge: Cambridge Univ. Press), 29
Guy Nir's code 2024, https://github.com/guynir42/earthshadow
Hambly, N. C., & Blair, A. 2024, RASTI, 3, 73
Hambly, N. C., MacGillivray, H. T., Read, M. A., et al. 2001, MNRAS, 326, 1279
Haqq-Misra, J., & Kopparapu, R. 2012, AcAau, 72, 15
Irureta-Goyena, B. Y., et al. 2025, PASP, 137, 054503
Knuth, K. H., Ailleris, P., Agrama, H. A., et al. 2025, Progress in Aerospace Sciences, 156, 101097, https://www.sciencedirect.com/science/article/abs/pii/S0376042125000235
Nir, G., Ofek, E. O., Ben-Ami, S., et al. 2021, MNRAS, 505, 2477
Solano, E., Villarroel, B., Rodrigo, C., et al. 2022, MNRAS, 515, 1380
Solano, E., Marcy, G., Villarroel, B., et al. 2023, MNRAS, 527, 6312
Teodorani, M. 2004, Journal of Scientific Exploration, 18, 217
Tokovinin, A. 2002, PASP, 114, 1156
Valdes, R. A., & Freitas, F., Jr. 1983, Icar, 53, 453
Vavilova, I. B., Pakulyak, L. K., Shlyapnikov, A. A., et al. 2012, KPCB, 28, 85
Vavilova, I. B., Yatskiv, Y. S., & Pakuliak, L. K. 2017, in IAU Symp. 325, Astroinformatics, Proc. Int. Astronomical Union (Cambridge: Cambridge Univ. Press), 361
Villarroel, B. 2024, The Vanishing Star Enigma and the 1952 Washington D. C. UFO Wave (Popular Science)
Villarroel, B., Imaz, I., & Bergstedt, J. 2016, AJ, 152, 76
Villarroel, B., Marcy, G. W., Geier, S., et al. 2021, NatSR, 11, 12794
Villarroel, B., Mattsson, L., Guergouri, H., et al. 2022a, AcAau, 194, 106
Villarroel, B., Pelckmans, K., Solano, E., et al. 2022b, Univ., 8, 561
Villarroel, B., Solano, E., & Marcy, G. W. 2025a, arXiv:2507.15896
Villarroel, B., Soodla, J., Comerón, S., et al. 2020, AJ, 159, 8
Villarroel, B., Watters, W. A., Streblyanska, A., Solano, E., & Geier, S. 2025b, MNRAS, in press
Waszczak, A., Prince, T. A., Laher, R., et al. 2017, PASP, 129, 034402